High-Resolution Positivity and Asymptotic Preserving Numerical Methods for Chemotaxis and Related Models

Alina Chertock and Alexander Kurganov

1 Introduction

Many microorganisms exhibit a special pattern formation at the presence of a chemoattractant, food, light or areas with high oxygen concentration; see, e.g. [51–53, 59, 73, 75, 81, 88–90]. Collective movement of cells and organisms in response to chemical gradients, *chemotaxis*, has attracted a lot of attention due to its critical role in a wide range of biological phenomena; see, e.g. [25], where detailed comparison between different chemotactic mechanisms is provided.

The classical PDE chemotaxis model was introduced by Patlak in [73] and Keller and Segel [51,52] and it is often referred to as the Patlak-Keller-Segel (PKS) model. The PKS model is derived at the macroscopic level in terms of the cell density and chemoattractant concentration and in the two-dimensional (2-D) case reads as

$$\begin{cases} \rho_t + \boldsymbol{\nabla}\cdot(\chi\rho\nabla c) = \mu\Delta\rho, \\ \tau c_t = \alpha\Delta c - \beta c + \gamma\rho, \end{cases} \tag{1}$$

where the cell density ρ and chemoattractant concentration c are functions of the spatial variables $\boldsymbol{x} = (x,y) \in \Omega \subset \mathbb{R}^2$ and time t, $\mu > 0$ and $\alpha > 0$ are diffusion coefficients, $\chi > 0$ is the chemotactic sensitivity constant, and the constants $\gamma > 0$ and $\beta > 0$ stand for the production and degradation rate of the chemoattractant, respectively. The constant τ determines the type of the system: It is parabolic-parabolic if $\tau = 1$ and parabolic-elliptic for $\tau = 0$.

Alina Chertock
Department of Mathematics and Center for Research in Scientific Computation, North Carolina State University, Raleigh, NC 27695, USA, e-mail: chertock@math.ncsu.edu

Alexander Kurganov
Department of Mathematics, Southern University of Science and Technology, Shenzhen, 518055, China and Mathematics Department, Tulane University, New Orleans, LA 70118, USA, e-mail: kurganov@math.tulane.edu

The PKS model (1) can be generalized to better describe the reality by taking into account several additional factors. For instance, one may consider a more realistic chemotactic sensitivity function $\chi = \chi(\rho, c)$ in the first equation of (1) as, e.g., in [42,51,62,89,90]. Some other factors, such as growth and death of cells, production and uptake of the chemoattractant by cells, presence of food and other chemicals in the system, may also be incorporated into the chemotaxis model, see, e.g., [89, 90]. We also refer the reader to [13,21,43–45,55,75], where several other modifications of the PKS system have been studied.

The most important phenomenon in chemotaxis is self-aggregation of cells (dramatic increase of ρ in a number of "centers"; see, e.g., [1,8,10,11,23,78,97]), which may occur even when the cells are initially distributed almost evenly over Ω. We note that the solution behavior depends on the value of the total mass, which under the assumption that no-flux boundary conditions are imposed, is conserved:

$$M := \int\limits_{\Omega} \rho(\boldsymbol{x},t)\,\mathrm{d}\boldsymbol{x} \equiv \int\limits_{\Omega} \rho(\boldsymbol{x},0)\,\mathrm{d}\boldsymbol{x}.$$

The behavior of the solutions of (1) also depends on the number of space dimensions. In the one-dimensional (1-D) case, global solutions exist for all initial conditions. In the 2-D case, the solution of (1) exists globally in time as long as the total mass M is initially below a critical threshold M_c. Otherwise, the solution may blow up in finite time; see, e.g., [12, 22, 36–39, 42, 44, 45, 49, 65, 75]. This blowup represents a mathematical description of the cell aggregation phenomenon that occurs in real biological systems; see, e.g., [1,8,10,11,22,23,67,78]. In the parabolic-elliptic case ($\tau = 0$), the critical mass values M_c are explicitly available, while this is not the case for the parabolic-parabolic system ($\tau = 1$); see, e.g., [75]. The density ρ of the blowing up solutions of (1) becomes a linear combination of several Dirac δ-functions plus a regular part; see, e.g., [22,40,66].

While the blowup and the formation of the δ-function are not an unreasonable modeling of the cell aggregation phenomenon, they create enormous and sometimes unnecessary challenges to both numerics and analysis. As a result, a number of regularizations of the PKS system (1) has been introduced in the literature. Many of the regularized models admit bounded, global-in-time solutions that approach *spiky* steady states as time increases. Most of the regularized chemotaxis models can be put into the following form:

$$\begin{cases} \rho_t + \nabla \cdot \big(g(\rho)\boldsymbol{Q}(\chi\nabla c)\big) = \mu\Delta\rho, \\ \tau c_t = \alpha\Delta c - \beta c + \gamma\rho, \end{cases} \tag{2}$$

where $g > 0$ and $\boldsymbol{Q} = (Q_1, Q_2)$ are smooth functions of their arguments; see, e.g., [21,43–45,55,62,69,76,80,95] and references therein. Some of the typical examples include a chemotaxis model with a saturated chemotactic flux, logistic, signal- and density-dependent sensitivity models, and others.

A model with saturated chemotactic flux was proposed in [21], where the following functions g and $\boldsymbol{Q}$ were taken:

$$g(\rho)=\rho,\quad \boldsymbol{Q}(\chi\nabla c)=\begin{cases}\chi\nabla c, & \text{if } |\nabla c|\le s^*,\\ \left(\dfrac{\chi|\nabla c|-s^*}{\sqrt{1+(\chi|\nabla c|-s^*)^2}}+s^*\right)\dfrac{\nabla c}{|\nabla c|}, & \text{otherwise.}\end{cases} \tag{3}$$

Here, s^* is a switching parameter, which defines small gradient values, for which the system (2), (3) reduces to the original PKS system (1) so that the effect of saturated chemotactic flux function is felt at large gradient regimes only. This is expected to result in solutions which are spiky but yet bounded for all times; see, e.g. [21, 55].

The signal- and density-dependent sensitivity models can be obtained, for instance, by taking

$$g(\rho)=\rho \quad \text{and} \quad \boldsymbol{Q}(\chi\nabla c)=\chi\frac{\nabla c}{(1+\kappa c)^2}$$

or

$$g(\rho)=\frac{\rho}{1+\kappa\rho} \quad \text{and} \quad \boldsymbol{Q}(\chi\nabla c)=\chi\nabla c,$$

respectively, where κ is a (small) regularization parameter and $\kappa\to 0$ leads to the original PKS system (1). A global classical solution exists for these models and the regularization parameter κ allows one to conduct a detailed bifurcation analysis and study pattern formation and properties of nonuniform solutions; see, e.g., [43,93,94] and references therein.

Generalizations of the PKS system (1) to multi-component chemotaxis models are also widely discussed in the literature; see, e.g., [29–31, 96] and references therein. In this case, a mathematical model for, say, two noncompetitive biological species is governed by the following system of PDEs:

$$\begin{cases}(\rho_1)_t+\nabla\cdot(g_1(\rho_1)\boldsymbol{Q}(\chi_1\nabla c))=\mu_1\Delta\rho_1,\\ (\rho_2)_t+\nabla\cdot(g_2(\rho_2)\boldsymbol{S}(\chi_2\nabla c)=\mu_2\Delta\rho_2,\\ \tau c_t=\alpha\Delta c-\beta c+\gamma_1\rho_1+\gamma_2\rho_2=0.\end{cases} \tag{4}$$

This model was proposed in [96] and then further studied both analytically [24, 29–33, 57] and numerically [16, 20, 55]. In (4), $\rho_1(\boldsymbol{x},t)$ and $\rho_2(\boldsymbol{x},t)$ denote the cell densities of the first and second species, $g_1>0$, $g_2>0$, $\boldsymbol{Q}=(Q_1,Q_2)$ and $\boldsymbol{S}=(S_1,S_2)$ are smooth functions of their arguments, $\chi_2>\chi_1>0$ are the chemotactic sensitivity constants, $\mu_1>0$ and $\mu_2>0$ are diffusion coefficients, and $\gamma_1>0$ and $\gamma_2>0$ are the production rates for the first and second species, respectively.

Similarly to the one-species PKS model, solutions of (4) may either remain smooth (with decaying maxima of both ρ_1 and ρ_2) or blow up in a finite time as it was proven in [29, 31]. Moreover, in some cases only simultaneous blowup is possible, while in others the theory fails to predict the behavior of the solution. In addition, in the blowup regime ρ_1 and ρ_2 may develop different types of singularities depending on the choice of functions g_1, g_2, $\boldsymbol{Q}$ and $\boldsymbol{S}$, values of χ_1 and χ_2 and on the total mass of each species:

$$M_1 := \int\limits_\Omega \rho_1(\boldsymbol{x},t)\,\mathrm{d}x\,\mathrm{d}y \quad \text{and} \quad M_2 := \int\limits_\Omega \rho_2(\boldsymbol{x},t)\,\mathrm{d}x\,\mathrm{d}y.$$

The classical PKS system (1) as well as the aforementioned related systems model the chemotaxis phenomenon on a macroscopic level. In many cases, this allows one to obtain a qualitatively accurate description of the chemotactic cell movement in an efficient way by solving the studied PDE models numerically. However, in certain practically relevant situations, a more accurate description may be required. Typically microscopic models are used, such as the Fokker-Planck equations, the Langevin equations or even some discrete particles models. We refer the reader to an overview paper [98] on collective behavior of active matter that includes swimming bacteria, chemotaxis effects, and many others; see also [6, 61, 74, 77].

In order to describe the chemotaxis at the cellular (microscopic) level, a class of Boltzmann-type kinetic equations has also been developed. A stochastic approach based on the velocity-jump process was introduced in [85] and was later used in the framework of kinetic chemotaxis models in [2, 70, 82]. The velocity-jump process characterizes the movement in two phases, namely, run and tumble. During the run phase, the cells move (almost) linearly with constant speed and in the tumble phase, they reorient their motion with a new velocity and direction. The resulting nondimensionalized Boltzmann-type kinetic equation reads as (see, e.g., [15, 41, 71]):

$$\begin{cases} \varepsilon f_t + \boldsymbol{v}\cdot\nabla_{\boldsymbol{x}} f = \dfrac{1}{\varepsilon}\displaystyle\int\limits_V \big(T[c]f' - T^*[c]f\big)\,\mathrm{d}\boldsymbol{v}', \\ \tau c_t = \alpha\Delta c - \beta c + \gamma\rho, \end{cases} \tag{5}$$

where $f := f_\varepsilon(\boldsymbol{x},t,\boldsymbol{v})$ is the probability density function (pdf) of cells at the position $\boldsymbol{x}$ with the velocity $\boldsymbol{v} = (u,v) \in \mathscr{V} \subset \mathbb{R}^2$ at a given time t, and $f' := f_\varepsilon(\boldsymbol{x},t,\boldsymbol{v}')$. In (5), $T[c]$ and $T^*[c]$ are the turning kernel operators, which describe the velocity change at $(\boldsymbol{x},t)$ from $\boldsymbol{v}'$ to $\boldsymbol{v}$ and from $\boldsymbol{v}$ to $\boldsymbol{v}'$, respectively, that is, $T[c] := T_\varepsilon[c](\boldsymbol{v},\boldsymbol{v}')$ and $T^*[c] := T_\varepsilon[c](\boldsymbol{v}',\boldsymbol{v})$, and ε is a nondimensional scaling parameter (mean-free path), which provides the ratio of the mean running length between jumps to the typical observation length scale. In this model, it is assumed that the tumble (the reorientation) is a Poisson process with rate $\int_{\mathscr{V}} T^*[c]\mathrm{d}\boldsymbol{v}'$ and that $T^*[c]/\int_{\mathscr{V}} T^*[c]\mathrm{d}\boldsymbol{v}'$ is the probability density for a change in velocity from $\boldsymbol{v}$ to $\boldsymbol{v}'$, given that a reorientation occurs for a cell at position $\boldsymbol{x}$, velocity $\boldsymbol{v}$, and time t; see, e.g., [15]. Notice that the microscopic pdf f is related to the macroscopic cell density ρ in the following way:

$$\rho(\boldsymbol{x},t) := \int\limits_{\mathscr{V}} f(\boldsymbol{x},t,\boldsymbol{v})\,\mathrm{d}\boldsymbol{v}. \tag{6}$$

The question of convergence (in the singular limit as $\varepsilon \to 0$) of the kinetic model (5) to the PKS system (1) has been extensively studied. More precisely, the global in time convergence was proven in the parabolic-elliptic case in [15]. In the parabolic-parabolic case, only local convergence results were established; see [48]. We also refer the reader to [71] for more results on the limiting process.

Solutions of the kinetic chemotaxis system (5) exhibit a behavior similar to those of the PKS system (1). They depend, however, not only on the value of the initial mass M, but also on the specific kernel T, whose choice is crucial in the kinetic chemotaxis modeling; see, e.g., [9,15]. At the same time, kinetic chemotaxis system may provide a more detailed description of the underlying cell dynamics and thus may be advantageous in a variety of applications.

While a large amount of effort has been expended on theoretical analysis of both macroscopic PDE and kinetic chemotaxis models over the past decades, the choice of numerical methods for these models is still rather limited. The main difficulty in numerical simulations of chemotaxis and related phenomena is associated with capturing blowing up or rapidly growing spiky solutions with high resolution and in an efficient manner.

Finite-volume [34] and finite-element [64, 79] methods were proposed for the PKS system (1) with the parabolic-elliptic ($\tau = 0$) coupling. A fractional step numerical method for fully time-dependent chemotaxis system from [90,97] was proposed in [91]. Such splitting approach may, however, not be applicable for the system (1) since its convective part may loose hyperbolicity. As it has been demonstrated in [18], the latter is a generic situation for the PKS model with parabolic-parabolic ($\tau = 1$) coupling. Several methods for the parabolic-parabolic PKS system have been recently proposed: a family of high-order discontinuous Galerkin methods has been designed in [27,28]; an implicit flux-corrected finite-element method has been developed in [84]. These methods achieve high-order of accuracy, but their high memory usage and computational costs are among their obvious drawbacks. Simpler and more efficient finite-volume and finite-volume-finite-difference methods were derived for the PKS system [16,18], two-species chemotaxis [16,55] and coupled chemotaxis-fluid models [17]. In [26], a modified version of the scheme from [18] is extended to the PKS system in irregular geometry using the upwind-difference potentials method. In [20], an adaptive moving mesh (AMM) finite-volume semi-discrete upwind method was developed and applied to two-species chemotaxis systems (4). Finally, several finite-volume methods have been recently introduced in [14,19,35] for 1-D and 2-D kinetic-chemotaxis systems (5) with different turning kernels.

It should be observed that due to the lack of hyperbolicity of the convective part in many chemotaxis systems, enforcing nonlinear stability of the designed numerical methods may be a very challenging task. Indeed, unlike many other models, in which appearance of unphysical (small) negative values is numerically tolerable, in the chemotaxis models negative, even small negative values of the cell density ρ, produced by a numerical method, will trigger the development of negative cell density spikes, which, in turn will make the computed solution completely irrelevant. Therefore, preserving positivity of the computed solutions is an absolutely crucial property a good numerical method as this is the only way to guarantee its nonlinear stability. It is quite easy to design first-order positivity preserving schemes, but first-order schemes are typically impractical due to low resolution and low efficiency. Deriving high-order (high-resolution) schemes that posses this property is a signifi-

cantly more complicated task, which was successfully achieved in a series of works presented in [16–18, 20, 21, 55].

In the context of kinetic-chemotaxis system (5), additional difficulty in designing an efficient and accurate numerical method is related to the fact that the underlying system is stiff when $0 < \varepsilon << 1$. If an explicit numerical discretization is used, one may need to take both spatial and temporal discretization parameters to be proportional to $\mathscr{O}(\varepsilon)$ or even $\mathscr{O}(\varepsilon^2)$ due to severe stability restrictions, which may become unaffordable for small ε. Implicit discretizations, which are often uniformly stable for $0 < \varepsilon < 1$, may, on the other hand, be inconsistent with the limit problem and provide a wrong solution in the $\varepsilon \to 0$ limit. In order to overcome this difficulty, the so-called asymptotic preserving (AP) schemes, which yield a consistent approximation of the limiting macroscopic PKS system as $\varepsilon \to 0$ and are stable on a coarse spatio-temporal grid with the mesh parameters being independent of ε have been recently introduced in [14, 19].

The goal of this review paper is to survey some of the recent advances in developing of high-resolution finite-volume and finite-difference numerical methods for chemotaxis-type systems that preserve positivity of the computed solutions and provide a consistent and stable discretization in certain asymptotic regimes.

The paper is organized as follows. In §2, we review positivity preserving hybrid finite-volume-finite-difference (FVFD) schemes. We begin in §2.1 with the second-order scheme, whose advantages and limitations are discussed and numerically illustrated in §2.1.1. The fourth-order FVFD scheme is presented in §2.2. Its advantages and disadvantages as well as additional moving-mesh resolution enhancement techniques are discussed in §2.2.1. In §3, we review the AP methods for kinetic-chemotaxis systems. In order to construct the AP methods, we use the odd-even formulation (§3.1), Strang operator splitting (§3.2), the exact ODE solver for the stiff subsystem (§3.3.1) and second-order upwinding for the nonstiff subsystem (§3.3.2). Finally, the AP property is proven in §3.4.

2 Positivity Preserving Finite-Volume-Finite-Difference Methods

In this section, we describe second- and fourth-order hybrid FVFD schemes, which were originally proposed in [16] for the PKS model (1), but we adapt the description to the more general system (2) (see also [17, 21, 55]). To this end, we introduce the chemotactic velocities $U := c_x$ and $V := c_y$ and rewrite (2) in the equivalent form:

$$\begin{cases} \rho_t + (g(\rho)Q_1(\chi U) - \mu\rho_x)_x + (g(\rho)Q_2(\chi V) - \mu\rho_y)_y = 0, \\ \tau c_t = \alpha\Delta c - \beta c + \gamma\rho. \end{cases} \tag{7}$$

Note that in the particular case of linear functions g and $\boldsymbol{Q} = (Q_1, Q_2)$, that is, if

$$g(\rho) = \rho, \quad Q_1(\chi U) = \chi U \quad \text{and} \quad Q_2(\chi V) = \chi V, \tag{8}$$

the system (7) reduces to the PKS system (1).

Before proceeding with the presentation of the numerical schemes for (7), it should be pointed out that preserving the positivity of the computed cell density ρ is very important since appearance of negative values may trigger numerical instabilities as it was demonstrated in [18]. Indeed, in near blowup regimes, the system (7) becomes convection-dominated and its convective part may loose hypervelocity. The latter can be illustrated by considering the parabolic-parabolic case ($\tau = 1$) and differentiating the second equation in (7) with respect to x and y and rewriting the system in the equivalent vector form as follows:

$$\begin{pmatrix}\rho\\U\\V\end{pmatrix}_t + \begin{pmatrix}g(\rho)Q_1(\chi U)\\-\gamma\rho\\0\end{pmatrix}_x + \begin{pmatrix}g(\rho)Q_2(\chi U)\\0\\-\gamma\rho\end{pmatrix}_y = \Delta\begin{pmatrix}\mu\rho\\\alpha U\\\alpha V\end{pmatrix} - \begin{pmatrix}0\\\beta U\\\beta V\end{pmatrix}. \quad (9)$$

One may now compute the x- and y-Jacobians of the convective fluxes, whose eigenvalues are given by

$$\left\{0,\ \frac{g'(\rho)Q_1(\chi U) \pm \sqrt{(g'(\rho)Q_1(\chi U))^2 - 4\gamma g(\rho)Q_1'(\chi U)}}{2}\right\},$$

and

$$\left\{0,\ \frac{g'(\rho)Q_2(\chi V) \pm \sqrt{(g'(\rho)Q_2(\chi V))^2 - 4\gamma g(\rho)Q_2'(\chi V)}}{2}\right\},$$

respectively. It is clear from the above calculations that the "purely" convective version of the systems (9),

$$\begin{pmatrix}\rho\\U\\V\end{pmatrix}_t + \begin{pmatrix}g(\rho)Q_1(\chi U)\\-\gamma\rho\\0\end{pmatrix}_x + \begin{pmatrix}g(\rho)Q_2(\chi U)\\0\\-\gamma\rho\end{pmatrix}_y = \mathbf{0}$$

is hyperbolic only if both

$$g'(\rho)Q_1(\chi U))^2 \geq 4\gamma g(\rho)Q_1'(\chi U) \quad \text{and} \quad g'(\rho)Q_2(\chi V))^2 \geq 4\gamma g(\rho)Q_2'(\chi V);$$

otherwise, it is elliptic. Unfortunately, the ellipticity condition is satisfied in generic cases, for example, when both g, Q_1 and Q_2 are linear functions (8), $U = V = 0$ and $\rho > 0$. Obviously, the complete chemotaxis system (9) contains stabilizing diffusion terms, but one has to be very careful since ellipticity of the convective part may still cause instabilities (especially if a fractional step approach is being implemented numerically).

It should also be emphasized that designing a positivity preserving second- and higher-order schemes is, in general, a nontrivial task and, to the best of our knowledge, the FVFD methods derived in [16] and presented below are among the first ones to achieve this goal for the chemotaxis system (7). In what follows we proceed with presenting these methods.

We consider the system (7) in a rectangular domain $\Omega \subset \mathbb{R}^2$, where we introduce a Cartesian mesh consisting of the cells $I_{j,k} := [x_{j-\frac{1}{2}}, x_{j+\frac{1}{2}}] \times [y_{k-\frac{1}{2}}, y_{k+\frac{1}{2}}]$, which, for the sake of simplicity, are assumed to be of the uniform size $|I_{j,k}| = \Delta x \Delta y$, that is, $x_{j+\frac{1}{2}} - x_{j-\frac{1}{2}} \equiv \Delta x$ for all j and $y_{k+\frac{1}{2}} - y_{k-\frac{1}{2}} \equiv \Delta y$ for all k. We assume that computed cell averages of ρ,

$$\overline{\rho}_{j,k}(t) := \frac{1}{|I_{j,k}|} \iint\limits_{I_{j,k}} \rho(x,y,t)\,\mathrm{d}x\mathrm{d}y,$$

and point values of the chemoattractant concentration, $c_{j,k}(t) \approx c(x_j, y_k, t)$ are available at a certain time level t (we will suppress the dependence of the indexed quantities on t in the subsequent text for the brevity of presentation unless it is required for clarity). These computed quantities are evolved in time according to a general semi-discrete hybrid FVFD scheme, which has the following form:

$$\begin{cases} \dfrac{\mathrm{d}\overline{\rho}_{j,k}}{\mathrm{d}t} = -\dfrac{\mathscr{F}_{j+\frac{1}{2},k} - \mathscr{F}_{j-\frac{1}{2},k}}{\Delta x} - \dfrac{\mathscr{G}_{j,k+\frac{1}{2}} - \mathscr{G}_{j,k-\frac{1}{2}}}{\Delta y}, \\ \tau \dfrac{\mathrm{d}c_{j,k}}{\mathrm{d}t} = \alpha \Delta_{j,k} c - \beta c_{j,k} + \gamma \rho_{j,k}. \end{cases} \tag{10}$$

Here, $\mathscr{F}_{j+\frac{1}{2},k}$ and $\mathscr{G}_{j,k+\frac{1}{2}}$ are the numerical fluxes in the x- and y-directions, respectively, $\Delta_{j,k}$ is a discrete Laplacian, and $\rho_{j,k}$ is an approximation of the point value of $\rho(x_j, y_k, t)$.

In the next sections, we will first provide the reader with a detailed description of both the second- and fourth-order versions of the FVFD scheme (10), including proofs of their positivity preserving property, and then present an AMM finite-volume method. These numerical schemes are obtained by different approximations of the numerical fluxes and discrete Laplacians in (10) and we will denote them by $\mathscr{F}^{\mathrm{II}}_{j+\frac{1}{2},k}$, $\mathscr{G}^{\mathrm{II}}_{j,k+\frac{1}{2}}$, $\Delta^{\mathrm{II}}_{j,k}$ and $\mathscr{F}^{\mathrm{IV}}_{j+\frac{1}{2},k}$, $\mathscr{G}^{\mathrm{IV}}_{j,k+\frac{1}{2}}$, $\Delta^{\mathrm{IV}}_{j,k}$ for the second- and fourth-order methods, respectively.

2.1 Second-Order Scheme

We approximate second-order numerical fluxes in (10),

$$\mathscr{F}^{\mathrm{II}}_{j+\frac{1}{2},k} = (gQ_1)^{\mathrm{II}}_{j+\frac{1}{2},k} - \mu(\rho_x)^{\mathrm{II}}_{j+\frac{1}{2},k} \text{ and } \mathscr{G}^{\mathrm{II}}_{j,k+\frac{1}{2}} = (gQ_1)^{\mathrm{II}}_{j+\frac{1}{2},k} - \mu(\rho_y)^{\mathrm{II}}_{j,k+\frac{1}{2}}, \tag{11}$$

using the central differences for the density derivatives:

$$(\rho_x)^{\mathrm{II}}_{j+\frac{1}{2},k} = \frac{\overline{\rho}_{j+1,k} - \overline{\rho}_{j,k}}{\Delta x}, \qquad (\rho_y)^{\mathrm{II}}_{j,k+\frac{1}{2}} = \frac{\overline{\rho}_{j,k+1} - \overline{\rho}_{j,k}}{\Delta y}, \tag{12}$$

and an upwind differencing scheme for the chemotactic fluxes:

$$(gQ_1)^{\rm II}_{j+\frac12,k}=\begin{cases}g(\rho^{\rm E}_{j,k})\,Q_1\big(\chi U^{\rm II}_{j+\frac12,k}\big), & \text{if } Q_1\big(\chi U^{\rm II}_{j+\frac12,k}\big)>0,\\ g(\rho^{\rm W}_{j+1,k})\,Q_1\big(\chi U^{\rm II}_{j+\frac12,k}\big), & \text{otherwise,}\end{cases}$$
$$(gQ_2)^{\rm II}_{j,k+\frac12}=\begin{cases}g(\rho^{\rm N}_{j,k})\,Q_2\big(\chi V^{\rm II}_{j,k+\frac12}\big), & \text{if } Q_2\big(\chi V^{\rm II}_{j,k+\frac12}\big)>0,\\ g(\rho^{\rm S}_{j,k+1})\,Q_2\big(\chi V^{\rm II}_{j,k+\frac12}\big), & \text{otherwise.}\end{cases}\tag{13}$$

In (13), the point values of the velocities are obtained by the central differences:

$$U^{\rm II}_{j+\frac12,k}=\frac{c_{j+1,k}-c_{j,k}}{\Delta x},\qquad V^{\rm II}_{j,k+\frac12}=\frac{c_{j,k+1}-c_{j,k}}{\Delta y},$$

and the one-sided point values at the cell interfaces, $\rho^{\rm E}_{j,k}$, $\rho^{\rm W}_{j+1,k}$, $\rho^{\rm N}_{j,k}$ and $\rho^{\rm S}_{j,k+1}$, are calculated from a second-order piecewise linear reconstruction

$$\widetilde{\rho}(x,y)=\overline{\rho}_{j,k}+(\rho_x)_{j,k}(x-x_j)+(\rho_y)_{j,k}(y-y_k),\quad (x,y)\in I_{j,k},\tag{14}$$

as follows:

$$\begin{aligned}\rho^{\rm E}_{j,k}&=\widetilde{\rho}(x_{j+\frac12}-0,y_k)=\overline{\rho}_{j,k}+\frac{\Delta x}{2}(\rho_x)^{\rm II}_{j,k},\\ \rho^{\rm W}_{j,k}&=\widetilde{\rho}(x_{j-\frac12}+0,y_k)=\overline{\rho}_{j,k}-\frac{\Delta x}{2}(\rho_x)^{\rm II}_{j,k},\\ \rho^{\rm N}_{j,k}&=\widetilde{\rho}(x_j,y_{k+\frac12}-0)=\overline{\rho}_{j,k}+\frac{\Delta y}{2}(\rho_y)^{\rm II}_{j,k},\\ \rho^{\rm S}_{j,k}&=\widetilde{\rho}(x_j,y_{k-\frac12}+0)=\overline{\rho}_{j,k}-\frac{\Delta y}{2}(\rho_y)^{\rm II}_{j,k}.\end{aligned}\tag{15}$$

It is important to guarantee nonnegativity of these reconstructed point values of ρ provided the computed cell averages $\overline{\rho}_{j,k}$ are nonnegative. One of the ways to achieve this goal is to use the following adaptive algorithm for computing the discrete slopes $(\rho_x)^{\rm II}_{j,k}$ and $(\rho_y)^{\rm II}_{j,k}$ in (15):

- Use central differences

$$(\rho_x)^{\rm II}_{j,k}=\frac{\overline{\rho}_{j+1,k}-\overline{\rho}_{j-1,k}}{2\Delta x},\qquad (\rho_y)^{\rm II}_{j,k}=\frac{\overline{\rho}_{j,k+1}-\overline{\rho}_{j,k-1}}{2\Delta y}$$

  to obtain the point values $\rho^{\rm E,W,N,S}_{j,k}$ in (15).

  If either $\rho^{\rm E}_{j,k}<0$ or $\rho^{\rm W}_{j,k}<0$, **then**

  Recompute these values by approximating the discrete derivative $(\rho_x)^{\rm II}_{j,k}$ in cell $I_{j,k}$ with the help of a positivity preserving nonlinear limiter. For instance, one can use the generalized minmod limiter [58, 60, 68, 86]:

$$(\rho_x)^{\rm II}_{j,k}=\text{minmod}\Big(2\,\frac{\overline{\rho}_{j+1,k}-\overline{\rho}_{j,k}}{\Delta x},\,\frac{\overline{\rho}_{j+1,k}-\overline{\rho}_{j-1,k}}{2\Delta x},\,2\,\frac{\overline{\rho}_{j,k}-\overline{\rho}_{j-1,k}}{\Delta x}\Big),$$

where

$$\text{minmod}(z_1,z_2,\ldots) := \begin{cases} \min(z_1,z_2,\ldots), & \text{if } z_i > 0 \ \forall i,\\ \max(z_1,z_2,\ldots), & \text{if } z_i < 0 \ \forall i,\\ 0, & \text{otherwise.}\end{cases}$$

If either $\rho^{\rm N}_{j,k} < 0$ or $\rho^{\rm S}_{j,k} < 0$, **then**

Recompute these values by approximating the discrete derivatives $(\rho_y)^{\rm II}_{j,k}$ in cell $I_{j,k}$ with the help of a positivity preserving nonlinear limiter. Once again, one can use, for example, the generalized minmod limiter:

$$(\rho_y)^{\rm II}_{j,k} = \text{minmod}\left(2\frac{\overline{\rho}_{j,k+1}-\overline{\rho}_{j,k}}{\Delta y}, \frac{\overline{\rho}_{j,k+1}-\overline{\rho}_{j,k-1}}{2\Delta y}, 2\frac{\overline{\rho}_{j,k}-\overline{\rho}_{j,k-1}}{\Delta y}\right).$$

This way, the positivity of reconstructed point values $\rho^{\rm E,W,N,S}_{j,k}$ will be guaranteed by the positivity preserving property of the chosen limiter. Besides the generalized minmod limiter, other positivity preserving limiters is are available in the literature; see, e.g., [58, 60, 68, 86].

Finally, the Laplace operator in (10) is approximated using the standard five-point stencil:

$$\Delta^{\rm II}_{j,k}c = \frac{c_{j+1,k}-2c_{j,k}+c_{j-1,k}}{(\Delta x)^2} + \frac{c_{j,k+1}-2c_{j,k}+c_{j,k-1}}{(\Delta y)^2},$$

the point values $\rho_{j,k}$ are approximated by the corresponding cell averages, and then the resulting second-order semi-discrete hybrid FVFD scheme reads as

$$\begin{cases} \dfrac{{\rm d}\overline{\rho}_{j,k}}{{\rm d}t} = -\dfrac{\mathscr{F}^{\rm II}_{j+\frac12,k}-\mathscr{F}^{\rm II}_{j-\frac12,k}}{\Delta x} - \dfrac{\mathscr{G}^{\rm II}_{j,k+\frac12}-\mathscr{G}^{\rm II}_{j,k-\frac12}}{\Delta y},\\ \tau\dfrac{{\rm d}c_{j,k}}{{\rm d}t} = \alpha\Delta^{\rm II}_{j,k}c - \beta c_{j,k} + \gamma\overline{\rho}_{j,k}.\end{cases} \tag{16}$$

The following theorems, proven in [16] for the PKS system (1), establish the positivity preserving property of the described numerical method in both the parabolic-parabolic ($\tau = 1$) and parabolic-elliptic ($\tau = 0$) cases. For the sake of completeness, we repeat the proof from [16] for a more general system (7).

Theorem 1. *Assume that the system of ODEs (16) with $\tau = 1$ is integrated using the forward Euler method:*

$$\begin{aligned}\overline{\rho}_{j,k}(t+\Delta t) = \overline{\rho}_{j,k}(t) &- \lambda\left(\mathscr{F}^{\rm II}_{j+\frac12,k}(t)-\mathscr{F}^{\rm II}_{j-\frac12,k}(t)\right)\\ &- \sigma\left(\mathscr{G}^{\rm II}_{j,k+\frac12}(t)-\mathscr{G}^{\rm II}_{j,k-\frac12}(t)\right),\end{aligned} \tag{17}$$

$$c_{j,k}(t+\Delta t) = (1-\beta\Delta t)c_{j,k}(t) + \alpha\Delta t\Delta^{\rm II}_{j,k}c_{j,k}(t) + \gamma\Delta t\overline{\rho}_{j,k}(t), \tag{18}$$

where $\lambda := \Delta t/\Delta x$ and $\sigma := \Delta t/\Delta y$. Then, the evolved cell densities $\overline{\rho}_{j,k}(t+\Delta t)$ and chemoattractant concentrations $c_{j,k}(t+\Delta t)$ will be nonnegative for all j,k pro-

vided $\overline{\rho}_{j,k}(t)$ and $c_{j,k}(t)$ are nonnegative for all j,k and the following CFL-like condition is satisfied:

$$\Delta t \le \min\left\{\frac{\Delta x}{8a}, \frac{\Delta y}{8b}, \frac{\Delta x\Delta y}{4K\mu}, \frac{1}{\max\{K_1,\delta\}}\right\}, \tag{19}$$

where

$$\begin{aligned} a &:= \max_{j,k}|Q_1(\chi U^{\mathrm{II}}_{j+\frac{1}{2},k})|\cdot\max_{j,k}\left\{\frac{g(\rho^{\mathrm{E}}_{j,k})}{\rho^{\mathrm{E}}_{j,k}}, \frac{g(\rho^{\mathrm{W}}_{j,k})}{\rho^{\mathrm{W}}_{j,k}}\right\},\\ b &:= \max_{j,k}|Q_2(\chi V^{\mathrm{II}}_{j,k+\frac{1}{2}})|\cdot\max_{j,k}\left\{\frac{g(\rho^{\mathrm{N}}_{j,k})}{\rho^{\mathrm{N}}_{j,k}}, \frac{g(\rho^{\mathrm{S}}_{j,k})}{\rho^{\mathrm{S}}_{j,k}}\right\},\\ K &:= \frac{\Delta x}{\Delta y}+\frac{\Delta y}{\Delta x}, \quad K_1 := \max_{j,k}\left(\beta+\frac{2K\alpha}{\Delta x\Delta y}-\gamma\overline{\rho}_{j,k}\right), \end{aligned} \tag{20}$$

and $\delta > 0$ is a small parameter.

Proof. We follow the lines of the positivity proof in [16, 18] and begin with the cell density equation (17). Recall that the positivity preserving property of the interpolant (14) will guarantee that the reconstructed point values $\rho^{\mathrm{E}}_{j,k}, \rho^{\mathrm{W}}_{j,k}, \rho^{\mathrm{N}}_{j,k}$ and $\rho^{\mathrm{S}}_{j,k}$ will be nonnegative provided $\overline{\rho}_{j,k}(t) \ge 0$, $\forall j,k$. We then use (11)–(13) and the conservation property for the cell densities, $\overline{\rho}_{j,k} = \frac{1}{8}(\rho^{\mathrm{E}}_{j,k}+\rho^{\mathrm{W}}_{j,k}+\rho^{\mathrm{S}}_{j,k}+\rho^{\mathrm{N}}_{j,k})+\frac{1}{2}\overline{\rho}_{j,k}$, to regroup the terms in (17) as follows:

$$\begin{aligned} \overline{\rho}_{j,k}(t+\Delta t) = &\left[\frac{1}{8}\rho^{\mathrm{W}}_{j,k}-\frac{\lambda}{2}\Big(|Q_1(\chi U^{\mathrm{II}}_{j-\frac{1}{2},k})|-Q_1(\chi U^{\mathrm{II}}_{j-\frac{1}{2},k})\Big)g(\rho^{\mathrm{W}}_{j,k})\right]\\ &+\left[\frac{1}{8}\rho^{\mathrm{E}}_{j,k}-\frac{\lambda}{2}\Big(|Q_1(\chi U^{\mathrm{II}}_{j+\frac{1}{2},k})|+Q_1(\chi U^{\mathrm{II}}_{j+\frac{1}{2},k})\Big)g(\rho^{\mathrm{E}}_{j,k})\right]\\ &+\frac{\lambda}{2}\Big[|Q_1(\chi U^{\mathrm{II}}_{j+\frac{1}{2},k})|-Q_1(\chi U^{\mathrm{II}}_{j+\frac{1}{2},k})\Big]g(\rho^{\mathrm{W}}_{j+1,k})\\ &+\frac{\lambda}{2}\Big[|Q_1(\chi U^{\mathrm{II}}_{j-\frac{1}{2},k})|+Q_1(\chi U^{\mathrm{II}}_{j-\frac{1}{2},k})\Big]g(\rho^{\mathrm{E}}_{j-1,k})\\ &+\left[\frac{1}{8}\rho^{\mathrm{S}}_{j,k}-\frac{\sigma}{2}\Big(|Q_2(\chi V^{\mathrm{II}}_{j,k-\frac{1}{2}})|-Q_2(\chi V^{\mathrm{II}}_{j,k-\frac{1}{2}})\Big)g(\rho^{\mathrm{S}}_{j,k})\right]\\ &+\left[\frac{1}{8}\rho^{\mathrm{N}}_{j,k}-\frac{\sigma}{2}\Big(|Q_2(\chi V^{\mathrm{II}}_{j,k+\frac{1}{2}})|+Q_2(\chi V^{\mathrm{II}}_{j,k+\frac{1}{2}})\Big)g(\rho^{\mathrm{N}}_{j,k})\right]\\ &+\frac{\sigma}{2}\Big[|Q_2(\chi V^{\mathrm{II}}_{j,k+\frac{1}{2}})|-Q_2(\chi V^{\mathrm{II}}_{j,k+\frac{1}{2}})\Big]g(\rho^{\mathrm{S}}_{j,k+1})\\ &+\frac{\sigma}{2}\Big[|Q_2(\chi V^{\mathrm{II}}_{j,k-\frac{1}{2}})|+Q_2(\chi V^{\mathrm{II}}_{j,k-\frac{1}{2}})\Big]g(\rho^{\mathrm{N}}_{j,k-1})+\left[\frac{1}{2}-\frac{2K\mu\Delta t}{\Delta x\Delta y}\right]\overline{\rho}_{j,k}(t)\\ &+\mu\Delta t\left[\frac{\overline{\rho}_{j+1,k}(t)+\overline{\rho}_{j-1,k}(t)}{(\Delta x)^2}+\frac{\overline{\rho}_{j,k+1}(t)+\overline{\rho}_{j,k-1}(t)}{(\Delta y)^2}\right]. \end{aligned} \tag{21}$$

As one can see from (21), $\overline{\rho}_{j,k}(t+\Delta t)$ is a linear combination of the five cell averages $\overline{\rho}_{j,k}(t)$, $\overline{\rho}_{j\pm1,k}(t)$, $\overline{\rho}_{j,k\pm1}(t)$ and eight point values $g(\rho^{\rm W}_{j,k})$, $g(\rho^{\rm E}_{j,k})$, $g(\rho^{\rm W}_{j+1,k})$, $g(\rho^{\rm E}_{j-1,k})$, $g(\rho^{\rm S}_{j,k})$, $g(\rho^{\rm N}_{j,k})$, $g(\rho^{\rm S}_{j,k+1})$, $g(\rho^{\rm N}_{j,k-1})$, which are all nonnegative since $g>0$ by assumption. The coefficients of this linear combination are also nonnegative under the CFL-like condition (19), which guarantees that $\overline{\rho}_{j,k}(t+\Delta t)\geq 0$ for all j,k.

Finally, the CFL-like condition (19) ensures that all of the terms on the right-hand side (RHS) of (18) are nonnegative and thus $c_{j,k}(t+\Delta t)\geq 0$ for all j,k, which completes the proof of the theorem. □

A similar theorem can be proven for the system of differential-algebraic equations (16) with $\tau=0$.

Theorem 2. *Assume that the first equation of the system of (16) with $\tau=0$ is integrated using the forward Euler method resulting in equation (17), while the system of linear algebraic equations for $c_{j,k}$ is solved exactly. Then, the evolved cell densities, $\overline{\rho}_{j,k}(t+\Delta t)$, and chemoattractant concentrations, $c_{j,k}(t+\Delta t)$, will be nonnegative for all j,k provided $\overline{\rho}_{j,k}(t)$ and $c_{j,k}(t)$ are nonnegative for all j,k and the following CFL-like condition is satisfied:*

$$\Delta t\leq \min\left\{\frac{\Delta x}{8a},\frac{\Delta y}{8b},\frac{\Delta x\Delta y}{4K\mu}\right\},\tag{22}$$

where a, b and K are given by (20).

Proof. The proof of this theorem follows the lines of the proof of Theorem 1 and the positivity of ρ is enforced the same way as in the parabolic-parabolic case, but with a different CFL-like condition as stated in the theorem. The difference in the CFL conditions is due to the fact that for $\tau=0$ the equation for the chemoattractant c reduces to a system of linear algebraic equations for $c_{j,k}$, which is to be solved by an accurate and efficient linear solver. It should be observed that the matrix of this linear system is diagonally dominant, which guarantees the positivity of c and no extra term is necessary in the CFL-like condition (22) compared to (19). □

Remark 1. Theorems 1 and 2 are also valid if the forward Euler method is replaced by a higher-order strong-stability preserving (SSP) ODE solver, since a time step in such solver can be written as a convex combination of several forward Euler steps.

Remark 2. It is instructive to point out that the upper bounds on the time step in (19) and (22) are minima of either four or three terms: the first two terms are related to the chemotactic fluxes, while the third and fourth ones are due to the diffusion and source terms there. In the (near) blowup regime, the system is convection-dominated, that is, the quantities a and b in (20) are large and thus the first two terms in (19) and (22) determine the size of time steps, in which case explicit methods are sufficiently efficient. However, when a and b are small, the third and fourth terms in (19) and (22) dominate and the efficiency of explicit methods is reduced. One of the ways to overcome this difficulty is to use implicit-explicit (IMEX) SSP methods (see, e.g., [4, 5, 47, 72]) as long as a and b remain relatively small. This does not affect the positivity preserving property of described method as was proven in [18].

2.1.1 Why Higher Resolution May Be Needed

In this section, we discuss advantages and limitations of the second-order hybrid FVFD scheme described in §2.1 and also demonstrate why higher-order/higher-resolution methods may be required to accurately compute solutions of chemotaxis systems. To this end, we will consider several numerical examples.

Example 1. We start by considering the PKS system (1) with

$$\tau = 0, \quad \chi = 20, \quad \mu = \alpha = \beta = \gamma = 1$$

and subject to the no-flux boundary conditions on $\Omega = [-3,3] \times [-3,3]$ and following initial condition:

$$\rho(x,y,0) = 100\, e^{-100(x^2+y^2)}.$$

According to the analytical results (see, e.g., [12,22,36–39,42,44,45,49,65,75]), the initial mass is above the critical one and therefore the solution is expected to blow up in finite time. In order to illustrate the blowup phenomenon, we compute the solution until the final time $t = 0.0038$ on a 101×101 uniform mesh. The obtained cell density is shown in Figure 1 (left). As one can see,

$$\|\rho^{101}(\cdot,\cdot,0.0038)\|_\infty \approx 559 \gg \|\rho(\cdot,\cdot,0)\|_\infty = 100,$$

which suggests that the solution may have already blown up by the final computational time. In order to verify this, we refine the mesh to 201×201 and observe that the maximum of the computed cell density shown in Figure 1 (right) is now

$$\|\rho^{201}(\cdot,\cdot,0.0038)\|_\infty \approx 2248 \approx 4 \times \|\rho^{101}(\cdot,\cdot,0.0038)\|_\infty.$$

This implies that the solution contains a δ-function, whose discrete maximum is supposed to be proportional to $1/(\Delta x \Delta y)$.

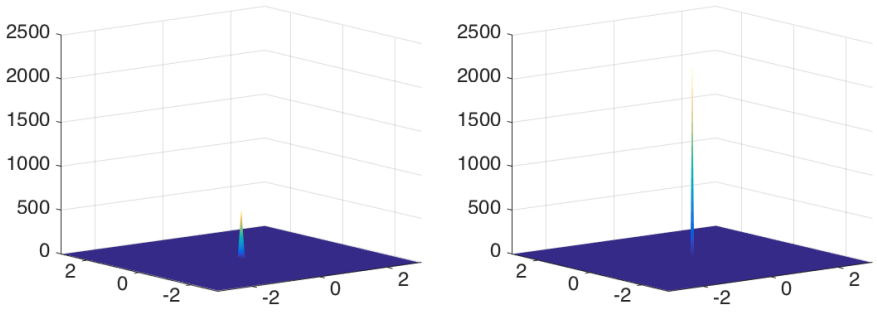

Fig. 1 Example 1: Cell density ρ computed using 101×101 (left) and 201×201 (right) meshes.

Comparing numerical solutions and its maximum norm on various meshes may allow one not only to confirm the solution blowup but also numerically predict the blowup time; see, e.g., [16]. The latter is an important piece of information, which may be required to be computed with a high precision and thus one may need to use a higher-order scheme and/or a certain adaptive strategy as an alternative to further mesh refinement study, which may become computationally unaffordable; see, e.g., [16, 20].

We would like to point out that even though using a higher-order or adaptive method in the initial-boundary value problem (IBVP) considered in Example 1 may enhance the achieved resolution, the second-order hybrid FVFD method seems to be sufficient to qualitatively understand the solution behavior (blowup). This may, however, not be the case in other situations like the one that will be considered in the second numerical example.

Example 2. We now consider the two-species chemotaxis system (4) with linear functions $g(\rho)=\rho$, $\boldsymbol{Q}(\chi_1\nabla c)=\chi_1\nabla c$ and $\boldsymbol{Q}(\chi_2\nabla c)=\chi_2\nabla c$, that is,

$$\tau=0,\quad \chi_1=1<\chi_2=20,\quad \mu_1=\mu_2=\alpha=\beta=\gamma_1=\gamma_2=1,$$

and subject to the no-flux boundary conditions on $\Omega=[-3,3]\times[-3,3]$ and following initial conditions:

$$\rho_1(x,y,0)=\rho_2(x,y,0)=50e^{-100(x^2+y^2)}.$$

Although the scheme in §2.1 was described for the one-species system (2), it can be straightforwardly extended to the two-species system (4) since the equations for ρ_1 and ρ_2 are only coupled through the c-equation. We note that a detailed description of the second-order hybrid FVFD scheme for the two-species model can be found in [55].

We compute the solution of the studied IBVP on a 201×201 uniform mesh. The cell densities ρ_1 and ρ_2 computed at time $t=0.0038$ are presented in Figure 2 (left column). As in Example 1, one can observe that the second-order FVFD scheme captures the spiky structure of the solution. However, one can clearly see the difference between the maximum values of ρ_1 and ρ_2:

$$\|\rho_1^{201}(\cdot,\cdot,0.0038)\|_\infty\approx30.26<\|\rho_1(\cdot,\cdot,0)\|_\infty=50,$$
$$\|\rho_2^{201}(\cdot,\cdot,0.0038)\|_\infty\approx646\gg\|\rho_2(\cdot,\cdot,0)\|_\infty=50,$$

which suggests that ρ_2 had blown up, while ρ_1 remained bounded as its magnitude, in fact, had decreased. One may want to verify this conjecture by refining the mesh. The results computed on a 401×401 uniform mesh are shown in Figure 2 (right column). The corresponding maximum values are now

$$\|\rho_1^{401}(\cdot,\cdot,0.0038)\|_\infty\approx34.05<\|\rho_1(\cdot,\cdot,0)\|_\infty=50,$$
$$\|\rho_2^{401}(\cdot,\cdot,0.0038)\|_\infty\approx2365\approx4\times\|\rho_2(\cdot,\cdot,0.0038)\|_\infty.$$

These computations seem to confirm the above conjecture. However, the analytical results proven in [29, 31] state that only simultaneous blowup is possible, which means that ρ_1 should also have blown up by $t = 0.0038$ though at a much slower rate than ρ_2. This means that the above conjecture, which was made solely based on the above second-order numerical results was wrong. Therefore, one would definitely need a higher-resolution method to obtain qualitatively more accurate results in this example.

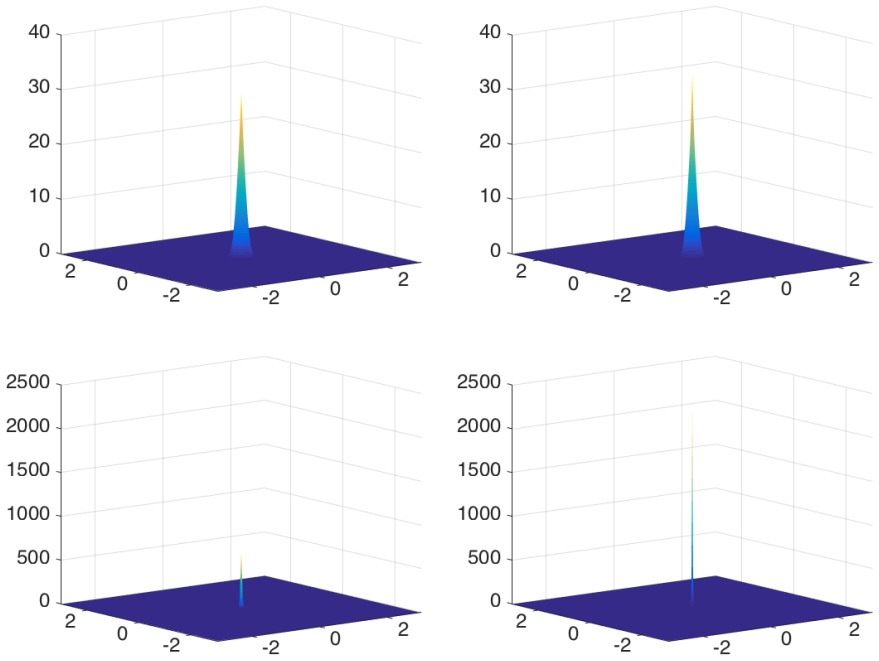

Fig. 2 Example 2: ρ_1 (top row) and ρ_2 (bottom row) computed using the second-order hybrid FVFD scheme on the 201×201 (left column) and 401×401 (right column) uniform meshes.

2.2 Fourth-Order Scheme

In this section, we describe the fourth-order hybrid FVFD scheme, which is a slightly improved version of the scheme that was derived in [16]. As it was mentioned above, we denote the fourth-order fluxes by

$$\mathscr{F}^{\mathrm{IV}}_{j+\frac{1}{2},k} = (gQ_1)^{\mathrm{IV}}_{j+\frac{1}{2},k} - \mu(\rho_x)^{\mathrm{IV}}_{j+\frac{1}{2},k} \quad \text{and} \quad \mathscr{G}^{\mathrm{IV}}_{j,k+\frac{1}{2}} = (gQ_2)^{\mathrm{IV}}_{j,k+\frac{1}{2}} - \mu(\rho_y)^{\mathrm{IV}}_{j,k+\frac{1}{2}}, \quad (23)$$

and approximate the density derivatives $(\rho_x)^{\rm IV}_{j+\frac12,k}$ and $(\rho_y)^{\rm IV}_{j,k+\frac12}$ in (23) using the fourth-order central differences:

$$(\rho_x)^{\rm IV}_{j+\frac12,k}=\frac{\overline{\rho}_{j-1,k}-15\overline{\rho}_{j,k}+15\overline{\rho}_{j+1,k}-\overline{\rho}_{j+2,k}}{12\Delta x},$$
$$(\rho_y)^{\rm IV}_{j,k+\frac12}=\frac{\overline{\rho}_{j,k-1}-15\overline{\rho}_{j,k}+15\overline{\rho}_{j,k+1}-\overline{\rho}_{j,k+2}}{12\Delta y}.$$

As in the second-order case, the chemotactic flux terms are computed in an upwind manner as follows:

$$(gQ_1)^{\rm IV}_{j+\frac12,k}=\begin{cases}\frac16\Big[g(\rho^{\rm NE}_{j,k})Q_1(\chi U^{\rm IV}_{j+\frac12,k+\frac12})+4g(\rho^{\rm E}_{j,k})Q_1(\chi U^{\rm IV}_{j+\frac12,k})\\ \quad+g(\rho^{\rm SE}_{j,k})Q_1(\chi U^{\rm IV}_{j+\frac12,k-\frac12})\Big],\quad \text{if } Q_1(\chi U^{\rm IV}_{j+\frac12,k})>0,\\ \frac16\Big[g(\rho^{\rm NW}_{j+1,k})Q_1(\chi U^{\rm IV}_{j+\frac12,k+\frac12})+4g(\rho^{\rm W}_{j+1,k})Q_1(\chi U^{\rm IV}_{j+\frac12,k})\\ \quad+g(\rho^{\rm SW}_{j+1,k})Q_1(\chi U^{\rm IV}_{j+\frac12,k-\frac12})\Big],\quad \text{otherwise,}\end{cases}$$
$$(gQ_2)^{\rm IV}_{j,k+\frac12}=\begin{cases}\frac16\Big[g(\rho^{\rm NW}_{j,k})Q_2(\chi V^{\rm IV}_{j-\frac12,k+\frac12})+4g(\rho^{\rm N}_{j,k})Q_2(\chi V^{\rm IV}_{j,k+\frac12})\\ \quad+g(\rho^{\rm NE}_{j,k})Q_2(\chi V^{\rm IV}_{j+\frac12,k+\frac12})\Big],\quad \text{if } Q_2(\chi V^{\rm IV}_{j,k+\frac12})>0,\\ \frac16\Big[g(\rho^{\rm SW}_{j,k+1})Q_2(\chi V^{\rm IV}_{j-\frac12,k+\frac12})+4g(\rho^{\rm S}_{j,k+1})Q_2(\chi V^{\rm IV}_{j,k+\frac12})\\ \quad+g(\rho^{\rm SE}_{j,k+1})Q_2(\chi V^{\rm IV}_{j+\frac12,k+\frac12})\Big],\quad \text{otherwise,}\end{cases}\tag{24}$$

where the velocities at the cell interfaces are obtained using the fourth-order central differences:

$$U^{\rm IV}_{j+\frac12,k}=\frac{c_{j-1,k}-27c_{j,k}+27c_{j+1,k}-c_{j+2,k}}{24\Delta x},$$
$$V^{\rm IV}_{j,k+\frac12}=\frac{c_{j,k-1}-27c_{j,k}+27c_{j,k+1}-c_{j,k+2}}{24\Delta y},\tag{25}$$

and the velocities at the cell vertices are obtained using the fourth-order averaging of the cell interface velocities (25), which results in

$$U^{\rm IV}_{j+\frac12,k+\frac12}=\frac{-U^{\rm IV}_{j+\frac12,k-1}+9U^{\rm IV}_{j+\frac12,k}+9U^{\rm IV}_{j+\frac12,k+1}-U^{\rm IV}_{j+\frac12,k+2}}{16},$$
$$V^{\rm IV}_{j+\frac12,k+\frac12}=\frac{-V^{\rm IV}_{j-1,k+\frac12}+9V^{\rm IV}_{j,k+\frac12}+9V^{\rm IV}_{j+1,k+\frac12}-V^{\rm IV}_{j+2,k+\frac12}}{16}.\tag{26}$$

Remark 3. We note that in [16], the velocities $U^{\mathrm{IV}}_{j+\frac12,k+\frac12}$ and $V^{\mathrm{IV}}_{j+\frac12,k+\frac12}$ were computed in a different manner. However, the formulae in (2.19) in [16] are not fully fourth-order and also computationally more expensive than (26).

In (24), the density point values along the cell interfaces, $\rho^{\mathrm{E}}_{j,k}$, $\rho^{\mathrm{W}}_{j,k}$, $\rho^{\mathrm{N}}_{j,k}$, $\rho^{\mathrm{S}}_{j,k}$, $\rho^{\mathrm{NE}}_{j,k}$, $\rho^{\mathrm{NW}}_{j,k}$, $\rho^{\mathrm{SE}}_{j,k}$ and $\rho^{\mathrm{SW}}_{j,k}$, are calculated using a conservative piecewise polynomial reconstruction

$$\begin{aligned}\mathscr{P}_{j,k}(x,y) = {}& \overline{\rho}_{j,k} + (\rho_x)_{j,k}(x-x_j) + (\rho_y)_{j,k}(y-y_k)\\ & \frac12(\rho_{xx})_{j,k}(x-x_j)^2 + (\rho_{xy})_{j,k}(x-x_j)(y-y_k) + \frac12(\rho_{yy})_{j,k}(y-y_k)^2\\ & \frac16(\rho_{xxx})_{j,k}(x-x_j)^3 + \frac12(\rho_{xxy})_{j,k}(x-x_j)^2(y-y_k)\\ & \frac12(\rho_{xyy})_{j,k}(x-x_j)(y-y_k)^2 + \frac16(\rho_{yyy})_{j,k}(y-y_k)^3\\ & \frac{1}{24}(\rho_{xxxx})_{j,k}(x-x_j)^4 + \frac14(\rho_{xxyy})_{j,k}(x-x_j)^2(y-y_k)^2\\ & \frac{1}{24}(\rho_{yyyy})_{j,k}(y-y_k)^4, \qquad (x,y)\in I_{j,k},\end{aligned}$$

which is almost fourth-order accurate provided its coefficients are obtained from the conservation requirements (see [54, Appendix B] for details):

$$\frac{1}{\Delta x\Delta y}\iint\limits_{I_{j+m,k+\ell}} \mathscr{P}_{j,k}(x,y)\,\mathrm{d}x\,\mathrm{d}y = \overline{\rho}_{j+m,k+\ell}, \quad \{m,\ell\in\mathbb{Z}:\,|m|+|\ell|\le 2\}.$$

The corresponding density point values are computed by (see [16] for detailed formulae and [54, Appendix B] for the algorithm of their efficient implementation)

$$\begin{aligned}\rho^{\mathrm{E}}_{j,k} &= \max\{\mathscr{P}_{j,k}(x_{j+\frac12},y_k),0\}, & \rho^{\mathrm{W}}_{j,k} &= \max\{\mathscr{P}_{j,k}(x_{j-\frac12},y_k),0\},\\ \rho^{\mathrm{N}}_{j,k} &= \max\{\mathscr{P}_{j,k}(x_j,y_{k+\frac12}),0\}, & \rho^{\mathrm{S}}_{j,k} &= \max\{\mathscr{P}_{j,k}(x_j,y_{k-\frac12}),0\},\\ \rho^{\mathrm{NE}}_{j,k} &= \max\{\mathscr{P}_{j,k}(x_{j+\frac12},y_{k+\frac12}),0\}, & \rho^{\mathrm{NW}}_{j,k} &= \max\{\mathscr{P}_{j,k}(x_{j-\frac12},y_{k+\frac12}),0\},\\ \rho^{\mathrm{SE}}_{j,k} &= \max\{\mathscr{P}_{j,k}(x_{j+\frac12},y_{k-\frac12}),0\}, & \rho^{\mathrm{SW}}_{j,k} &= \max\{\mathscr{P}_{j,k}(x_{j-\frac12},y_{k-\frac12}),0\},\end{aligned}$$

whose nonnegativity is enforced in the most straightforward way.

Equipped with the above quantities, we obtain the following (almost) fourth-order semi-discrete hybrid FVFD scheme:

$$\begin{cases}\dfrac{\mathrm{d}\overline{\rho}_{j,k}}{\mathrm{d}t} = -\dfrac{\mathscr{F}^{\mathrm{IV}}_{j+\frac12,k}-\mathscr{F}^{\mathrm{IV}}_{j-\frac12,k}}{\Delta x} - \dfrac{\mathscr{G}^{\mathrm{IV}}_{j,k+\frac12}-\mathscr{G}^{\mathrm{IV}}_{j,k-\frac12}}{\Delta y},\\ \tau\dfrac{\mathrm{d}c_{j,k}}{\mathrm{d}t} = \alpha\Delta^{\mathrm{IV}}_{j,k}c - \beta c_{j,k} + \gamma\rho_{j,k},\end{cases} \tag{27}$$

where a nine-point stencil is used to compute a fourth-order approximate Laplace operator,

$$\begin{aligned}\Delta^{\rm IV}_{j,k}c=&\frac{-c_{j-2,k}+16c_{j-1,k}-30c_{j,k}+16c_{j+1,k}-c_{j+2,k}}{12(\Delta x)^2}\\&+\frac{-c_{j,k-2}+16c_{j,k-1}-30c_{j,k}+16c_{j,k+1}-c_{j,k+2}}{12(\Delta y)^2},\end{aligned}\tag{28}$$

and $\rho_{j,k}=\max\{\mathscr{P}_{j,k}(x_j,y_k),0\}$ are point values of ρ at the centers of cells $I_{j,k}$.

As in the case of the second-order method, the fourth-order FVFD scheme (27) is either a system of ODEs ($\tau=1$) or differential-algebraic equations ($\tau=0$) and should be integrated in time by a sufficiently accurate and stable ODE solver. We recall that the positivity preserving property of the second-order method was enforced by both the positivity of the reconstructed point values of the density and a proper choice of the ODE solver and its time step. Unfortunately, this is not the case here: even if one uses an SSP ODE solver, positivity of ρ and c cannot be guaranteed.

One of the ways to ensure that the computed solution will remain nonnegative at all times is to adapt the so-called "draining" time step strategy, which was originally proposed in [7] in the context of the Saint-Venant system of shallow water equations. This approach, which is described below for the forward Euler time discretization, is based on the idea of locally limiting the outgoing fluxes at cells where negative solution values appear.

We start by considering the parabolic-parabolic case ($\tau=1$) and reformulate the fourth-order Laplacian in (28) in terms of diffusion fluxes as follows:

$$\alpha\Delta^{\rm IV}_{j,k}c=-\frac{\mathscr{H}^{\rm IV}_{j+\frac12,k}-\mathscr{H}^{\rm IV}_{j-\frac12,k}}{\Delta x}-\frac{\mathscr{L}^{\rm IV}_{j,k+\frac12}-\mathscr{L}^{\rm IV}_{j,k-\frac12}}{\Delta y}$$

where

$$\begin{aligned}\mathscr{H}^{\rm IV}_{j+\frac12,k}&=\alpha\,\frac{-c_{j-1,k}+15c_{j,k}-15c_{j+1,k}+c_{j+2,k}}{12\Delta x},\\ \mathscr{L}^{\rm IV}_{j,k+\frac12}&=\alpha\,\frac{-c_{j,k-1}+15c_{j,k}-15c_{j,k+1}+c_{j,k+2}}{12\Delta y}.\end{aligned}$$

We then rewrite the fourth-order semi-discrete hybrid FVFD scheme (27) in the following flux form:

$$\begin{cases}\dfrac{{\rm d}\overline{\rho}_{j,k}}{{\rm d}t}=-\dfrac{\mathscr{F}^{\rm IV}_{j+\frac12,k}-\mathscr{F}^{\rm IV}_{j-\frac12,k}}{\Delta x}-\dfrac{\mathscr{G}^{\rm IV}_{j,k+\frac12}-\mathscr{G}^{\rm IV}_{j,k-\frac12}}{\Delta y},\\[2ex]\dfrac{{\rm d}c_{j,k}}{{\rm d}t}=-\dfrac{\mathscr{H}^{\rm IV}_{j+\frac12,k}-\mathscr{H}^{\rm IV}_{j-\frac12,k}}{\Delta x}-\dfrac{\mathscr{L}^{\rm IV}_{j,k+\frac12}-\mathscr{L}^{\rm IV}_{j,k-\frac12}}{\Delta y}-\beta c_{j,k}+\gamma\rho_{j,k},\end{cases}\tag{29}$$

and evolve the numerical solution in time using the forward Euler discretization of (29):

$$\overline{\rho}_{j,k}(t+\Delta t) = \overline{\rho}_{j,k}(t) - \lambda\left(\widehat{\mathscr{F}}^{\mathrm{IV}}_{j+\frac{1}{2},k}(t) - \widehat{\mathscr{F}}^{\mathrm{IV}}_{j-\frac{1}{2},k}(t)\right) - \sigma\left(\widehat{\mathscr{G}}^{\mathrm{IV}}_{j,k+\frac{1}{2}}(t) - \widehat{\mathscr{G}}^{\mathrm{IV}}_{j,k-\frac{1}{2}}(t)\right), \tag{30}$$

$$\begin{aligned} c_{j,k}(t+\Delta t) &= (1-\beta\Delta t)c_{j,k}(t) + \gamma\Delta t\rho_{j,k}(t) \\ &\quad - \lambda\left(\widehat{\mathscr{H}}^{\mathrm{IV}}_{j+\frac{1}{2},k}(t) - \widehat{\mathscr{H}}^{\mathrm{IV}}_{j-\frac{1}{2},k}(t)\right) - \sigma\left(\widehat{\mathscr{L}}^{\mathrm{IV}}_{j,k+\frac{1}{2}}(t) - \widehat{\mathscr{L}}^{\mathrm{IV}}_{j,k-\frac{1}{2}}(t)\right), \end{aligned} \tag{31}$$

where $\lambda := \Delta t/\Delta x$, $\sigma := \Delta t/\Delta y$ and $\widehat{\mathscr{F}}^{\mathrm{IV}}_{j+\frac{1}{2},k}$, $\widehat{\mathscr{G}}^{\mathrm{IV}}_{j,k+\frac{1}{2}}$, $\widehat{\mathscr{H}}^{\mathrm{IV}}_{j+\frac{1}{2},k}$ and $\widehat{\mathscr{L}}^{\mathrm{IV}}_{j,k+\frac{1}{2}}$ are modified numerical fluxes defined as follows:

$$\begin{aligned} \widehat{\mathscr{F}}^{\mathrm{IV}}_{j+\frac{1}{2},k} &= \frac{\Delta t^{\rho}_{j+\frac{1}{2},k}}{\Delta t}\mathscr{F}^{\mathrm{IV}}_{j+\frac{1}{2},k}, \quad \widehat{\mathscr{G}}^{\mathrm{IV}}_{j,k+\frac{1}{2}} = \frac{\Delta t^{\rho}_{j,k+\frac{1}{2}}}{\Delta t}\mathscr{G}^{\mathrm{IV}}_{j,k+\frac{1}{2}} \\ \widehat{\mathscr{H}}^{\mathrm{IV}}_{j+\frac{1}{2},k} &= \frac{\Delta t^{c}_{j+\frac{1}{2},k}}{\Delta t}\mathscr{H}^{\mathrm{IV}}_{j+\frac{1}{2},k}, \quad \widehat{\mathscr{L}}^{\mathrm{IV}}_{j,k+\frac{1}{2}} = \frac{\Delta t^{c}_{j,k+\frac{1}{2}}}{\Delta t}\mathscr{L}^{\mathrm{IV}}_{j,k+\frac{1}{2}}. \end{aligned} \tag{32}$$

The time step Δt and the coefficients in front of the numerical fluxes in (32) are obtained according to following algorithm:

- Compute Δt according to the CFL-like condition (19).
- Compute "draining" time steps:

$$\begin{aligned} \Delta t^{\rho}_{j,k} &:= \frac{\Delta x\Delta y\overline{\rho}_{j,k}(t)}{f^{\rho}_{j,k}\Delta y + g^{\rho}_{j,k}\Delta x}, \\ \Delta t^{c}_{j,k} &:= \frac{\Delta x\Delta y[(1-\beta\Delta t)c_{j,k}(t) + \gamma\Delta t\rho_{j,k}(t)]}{f^{c}_{j,k}\Delta y + g^{c}_{j,k}\Delta x}, \end{aligned} \tag{33}$$

  where

$$\begin{aligned} f^{\rho}_{j,k} &:= \max(\mathscr{F}^{\mathrm{IV}}_{j+\frac{1}{2},k},0) + \max(-\mathscr{F}^{\mathrm{IV}}_{j-\frac{1}{2},k},0), \\ g^{\rho}_{j,k} &:= \max(\mathscr{G}^{\mathrm{IV}}_{j,k+\frac{1}{2}},0) + \max(-\mathscr{G}^{\mathrm{IV}}_{j,k-\frac{1}{2}},0), \\ f^{c}_{j,k} &:= \max(\mathscr{H}^{\mathrm{IV}}_{j+\frac{1}{2},k},0) + \max(-\mathscr{H}^{\mathrm{IV}}_{j-\frac{1}{2},k},0), \\ g^{c}_{j,k} &:= \max(\mathscr{L}^{\mathrm{IV}}_{j,k+\frac{1}{2}},0) + \max(-\mathscr{L}^{\mathrm{IV}}_{j,k-\frac{1}{2}},0). \end{aligned} \tag{34}$$

- Use the computed values of Δt and "draining" time steps to obtain

$$\begin{aligned} \Delta t^{\rho}_{j+\frac{1}{2},k} &:= \min(\Delta t, \Delta t^{\rho}_{m,k}), \quad m = j + \frac{1}{2} - \frac{\mathrm{sgn}(\mathscr{F}^{\mathrm{IV}}_{j+\frac{1}{2},k})}{2}, \\ \Delta t^{\rho}_{j,k+\frac{1}{2}} &:= \min(\Delta t, \Delta t^{\rho}_{j,\ell}), \quad \ell = k + \frac{1}{2} - \frac{\mathrm{sgn}(\mathscr{G}^{\mathrm{IV}}_{j,k+\frac{1}{2}})}{2}, \\ \Delta t^{c}_{j+\frac{1}{2},k} &:= \min(\Delta t, \Delta t^{c}_{p,k}), \quad p = j + \frac{1}{2} - \frac{\mathrm{sgn}(\mathscr{H}^{\mathrm{IV}}_{j+\frac{1}{2},k})}{2}, \\ \Delta t^{c}_{j,k+\frac{1}{2}} &:= \min(\Delta t, \Delta t^{c}_{j,q}), \quad q = k + \frac{1}{2} - \frac{\mathrm{sgn}(\mathscr{L}^{\mathrm{IV}}_{j,k+\frac{1}{2}})}{2}. \end{aligned} \tag{35}$$

In the parabolic-elliptic ($\tau = 0$) case, the second equation in (27) reduces to a system of linear (time-independent) algebraic equations for $c_{j,k}$, which, as in the second-order method, is to be solved by an accurate and efficient linear algebra solver. However, the matrix of this linear system is no longer diagonally dominant, and thus the positivity of c cannot not be in general guaranteed. On the other hand, the following theorem from [16] establishes the nonnegativity of the computed ρ and c at all times in the parabolic-parabolic ($\tau = 1$) case and we repeat its proof here for the sake of completeness.

Theorem 3. *Assume that the system of ODEs (29) is integrated using the forward Euler method (30)–(35). Then, the evolved cell densities $\overline{\rho}_{j,k}(t+\Delta t)$ and chemoattractant concentrations $c_{j,k}(t+\Delta t)$ remain nonnegative for all j,k as long as $\overline{\rho}_{j,k}(t)$ and $c_{j,k}(t)$ are nonnegative for all j,k.*

Proof. In order to prove the nonnegativity of ρ, one needs to consider different cases depending on the sign of the fluxes $\mathscr{F}^{\rm IV}_{j+\frac{1}{2},k}$ and $\mathscr{G}^{\rm IV}_{j,k+\frac{1}{2}}$ given by (23). We will only consider one of these cases, namely, assuming that

$$\mathscr{F}^{\rm IV}_{j+\frac{1}{2},k} > 0, \quad \mathscr{F}^{\rm IV}_{j-\frac{1}{2},k} > 0 \quad \text{and} \quad \mathscr{G}^{\rm IV}_{j,k+\frac{1}{2}} < 0, \quad \mathscr{G}^{\rm IV}_{j,k-\frac{1}{2}} < 0. \tag{36}$$

in the cell $I_{j,k}$. All of the other cases can be analyzed in a similar way.

First, we use the definitions in (34) to obtain

$$f^{\rho}_{j,k} = \mathscr{F}^{\rm IV}_{j+\frac{1}{2},k}, \quad g^{\rho}_{j,k} = -\mathscr{G}^{\rm IV}_{j,k-\frac{1}{2}}, \tag{37}$$

and then substituting (37) into (33) results in

$$\Delta t^{\rho}_{j,k} = \frac{\Delta x \Delta y \overline{\rho}_{j,k}(t)}{\mathscr{F}^{\rm IV}_{j+\frac{1}{2},k}\Delta y - \mathscr{G}^{\rm IV}_{j,k-\frac{1}{2}}\Delta x} > 0. \tag{38}$$

It also follows from (36) and (35) that

$$\begin{aligned}
&\Delta t^{\rho}_{j+\frac{1}{2},k} = \min(\Delta t, \Delta t^{\rho}_{j,k}), \qquad \Delta t^{\rho}_{j-\frac{1}{2},k} = \min(\Delta t, \Delta t^{\rho}_{j-1,k}),\\
&\Delta t^{\rho}_{j,k+\frac{1}{2}} = \min(\Delta t, \Delta t^{\rho}_{j,k+1}), \quad \Delta t^{\rho}_{j,k-\frac{1}{2}} = \min(\Delta t, \Delta t^{\rho}_{j,k}).
\end{aligned}$$

We now rewrite equation (30) as

$$\begin{aligned}
\overline{\rho}_{j,k}(t+\Delta t) = \overline{\rho}_{j,k}(t) &+ \frac{\Delta t^{\rho}_{j-\frac{1}{2},k}}{\Delta x}\mathscr{F}^{\rm IV}_{j-\frac{1}{2},k} - \frac{\Delta t^{\rho}_{j,k+\frac{1}{2}}}{\Delta y}\mathscr{G}^{\rm IV}_{j,k+\frac{1}{2}}\\
&+ \frac{\Delta t^{\rho}_{j,k-\frac{1}{2}}}{\Delta y}\mathscr{G}^{\rm IV}_{j,k-\frac{1}{2}} - \frac{\Delta t^{\rho}_{j+\frac{1}{2},k}}{\Delta x}\mathscr{F}^{\rm IV}_{j+\frac{1}{2},k},
\end{aligned} \tag{39}$$

and show that the RHS of (39) is nonnegative. To this end, we first note that (36) implies

$$\frac{\Delta t^{\rho}_{j-\frac{1}{2},k}}{\Delta x}\mathscr{F}^{\mathrm{IV}}_{j-\frac{1}{2},k}-\frac{\Delta t^{\rho}_{j,k+\frac{1}{2}}}{\Delta y}\mathscr{G}^{\mathrm{IV}}_{j,k+\frac{1}{2}}>0. \tag{40}$$

We then note that $\Delta t^{\rho}_{j+\frac{1}{2},k}=\Delta t^{\rho}_{j,k-\frac{1}{2}}\le\Delta t^{\rho}_{j,k}$, and therefore using (38), (39) and (40), we conclude with

$$\begin{aligned}\overline{\rho}_{j,k}(t+\Delta t)&>\overline{\rho}_{j,k}(t)+\frac{\Delta t^{\rho}_{j,k-\frac{1}{2}}}{\Delta y}\mathscr{G}^{\mathrm{IV}}_{j,k-\frac{1}{2}}-\frac{\Delta t^{\rho}_{j+\frac{1}{2},k}}{\Delta x}\mathscr{F}^{\mathrm{IV}}_{j+\frac{1}{2},k}\\&\ge\overline{\rho}_{j,k}(t)+\frac{\Delta x\overline{\rho}_{j,k}(t)}{\mathscr{F}^{\mathrm{IV}}_{j+\frac{1}{2},k}\Delta y-\mathscr{G}^{\mathrm{IV}}_{j,k-\frac{1}{2}}\Delta x}\mathscr{G}^{\mathrm{IV}}_{j,k-\frac{1}{2}}-\frac{\Delta y\overline{\rho}_{j,k}(t)}{\mathscr{F}^{\mathrm{IV}}_{j+\frac{1}{2},k}\Delta y-\mathscr{G}^{\mathrm{IV}}_{j,k-\frac{1}{2}}\Delta x}\mathscr{F}^{\mathrm{IV}}_{j+\frac{1}{2},k}=0,\end{aligned}$$

which shows that $\overline{\rho}_{j,k}(t+\Delta t)\ge 0$ for all j,k, provided that $\overline{\rho}_{j,k}(\Delta t)\ge 0$ for all j,k.

The nonnegativity proof for the c component of the solution can be obtained similarly, and the proof of the theorem will be completed. □

Remark 4. Note that the positivity preserving property of the second-order scheme can be also enforced using the "draining" time step technique instead of the adaptive reconstruction approach implemented in §2.1.

Remark 5. As an alternative way of achieving the positivity preserving property of fourth- and higher-order methods, one cam implement a maximum-principle-satisfying approach developed in [99] in the context of scalar conservation laws.

2.2.1 What Can Be Achieved with Higher-Resolution Methods

As it was mentioned in §2.1.1, capturing fast growing and/or singular solutions of chemotaxis systems is a challenging task. Example 2 as well as studies conducted in a series of works, [14, 16, 20, 55] clearly illustrate that in some cases under-resolved numerical simulations may lead to very misleading results in terms of determining blowup regimes of the computed solutions. In many of such cases, including the two-spices chemotaxis models like (4), where different blowup time scales are exhibited by the two variables, a very fine mesh (often practically unaffordable) would typically be required to make a blowup conjecture based on the numerical results even if the aforementioned fourth-order FVFD method is implemented as demonstrated in the following example; see also [16, 20, 55].

Example 3. We now consider the same IBVP for two-species chemotaxis system as in Example 2 and numerically solve it using the hybrid fourth-order FVFD scheme described in §2.2, which, similarly to its second-order counterpart, can be straightforwardly extended to the two-species system.

As in Example 2, we first compute the solution of the studied IBVP on a 201×201 uniform mesh. The cell densities ρ_1 and ρ_2 computed at time $t=0.0038$ are

presented in Figure 3 (left column). Once again, we observe that the maximum values of the computed ρ_1 and ρ_2,

$$\|\rho_1^{201}(\cdot,\cdot,0.0038)\|_\infty \approx 36.18 < \|\rho_1(\cdot,\cdot,0)\|_\infty = 50,$$
$$\|\rho_2^{201}(\cdot,\cdot,0.0038)\|_\infty \approx 2104 \gg \|\rho_2(\cdot,\cdot,0)\|_\infty = 50,$$

clearly indicate that ρ_2 blows up. In fact, its maximum is substantially larger than the one obtained by the second-order scheme in Example 2. However, it is hard (or even impossible) to draw a blowup conclusion about ρ_1, whose maximum is still below the initial one though it is larger than the maximum of ρ_1 computed using the 401×401 uniform meshes reported in Example 2. We then refine the mesh. The results computed on a 401×401 uniform mesh are shown in Figure 3 (right column). The corresponding maximum values are now

$$\|\rho_1^{401}(\cdot,\cdot,0.0038)\|_\infty \approx 42.25 < \|\rho_1(\cdot,\cdot,0)\|_\infty = 50,$$
$$\|\rho_2^{401}(\cdot,\cdot,0.0038)\|_\infty \approx 8284 \approx 4\times\|\rho_2(\cdot,\cdot,0.0038)\|_\infty.$$

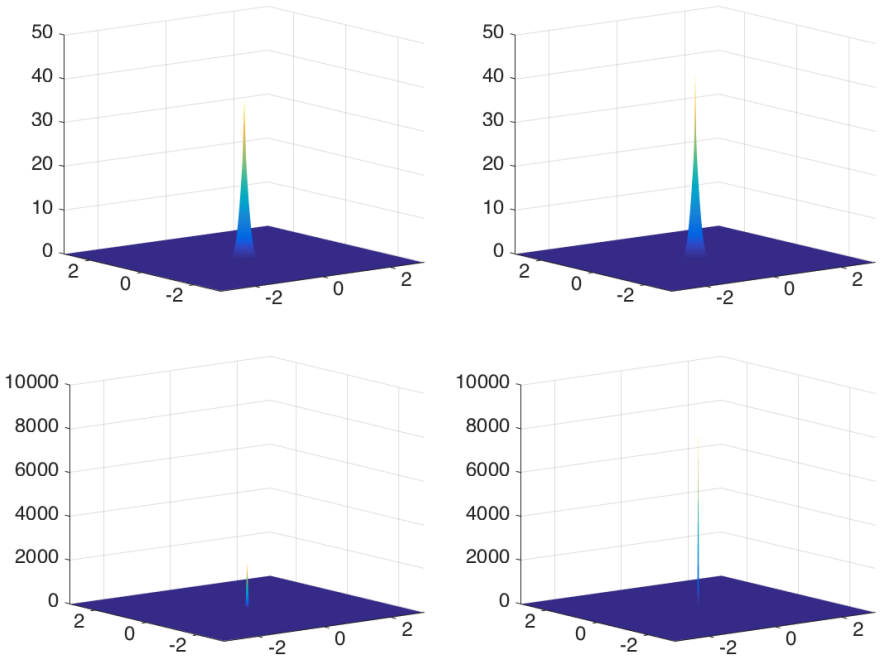

Fig. 3 Example 3: ρ_1 (top row) and ρ_2 (bottom row) computed using the fourth-order hybrid FVFD scheme on the 201×201 (left column) and 401×401 (right column) uniform meshes.

These computations demonstrate that the required resolution has not been achieved yet. One therefore may want to further increase the order of the numerical method. This, however, may be quite cumbersome and also computationally expensive. In addition, implementing higher-order boundary conditions may also be challenging.

As an alternative approach of enhancing the resolution of spiky solutions in the concentration/blowup regions, one may use an adaptive technique. For example, an adaptive moving mesh (AMM) method was proposed in [20] for the two-spices parabolic-elliptic chemotaxis system (4) with $\tau = 0$ by combining the second-order positivity preserving finite-volume method with the AMM technique from [56]. A general algorithm of the AMM approach consists of the evolution, mesh adaptation and projection steps. In particular, the solution is first evolved to the new time level on a given structured quadrilateral mesh. The mesh is then adapted to reflect the structure of the evolved solution and finally, the solution is projected onto the new mesh in a conservative manner. For more information about the AMM approach we refer the reader to [3, 46, 56, 87] and references therein.

In order to illustrate the performance of the AMM method, we apply it to the aforementioned IBVP using 101×101 adaptively moving cells. The obtained results are reported in Figure 4 and the maximum values of ρ_1 and ρ_2 are 62.38 and 622178. As one can see, the maximum value of ρ_2 is now much larger even than the one computed using the fourth-order FVFD scheme on the 401×401 uniform mesh. The maximum value of ρ_1 is now larger than the maximum if the initial datum, which suggests that ρ_1 may develop a sharp spiky structure even though one still cannot draw a definite conclusion whether the computed ρ_1 had blown up.

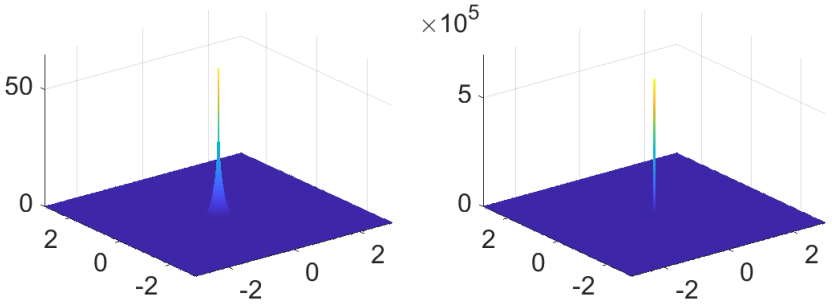

Fig. 4 Example 3: ρ_1 (left) and ρ_2 (right) computed using the second-order AMM finite-volume method 101×101 adaptively moving cells.

3 Asymptotic Preserving Methods

In this section, we consider the kinetic chemotaxis models (5) and describe how consistent and stable methods, whose properties are independent of ε can be derived.

As it was mentioned above, the choice of the turning kernel T in (5) plays a crucial role in chemotaxis modeling and we start by assuming that the turning kernel has an asymptotic expansion of the form (see, e.g., [14, 15, 35, 41, 71]):

$$T[c] = T_0[c] + \varepsilon T_1[c] + \mathscr{O}(\varepsilon^2). \tag{41}$$

Here, the leading term $T_0[c] = F(\boldsymbol{v}) > 0$ is the bounded velocity distribution at the equilibrium, which satisfies the following assumptions:

$$\int\limits_{\mathscr{V}} F(\boldsymbol{v})\,\mathrm{d}\boldsymbol{v} = 1 \quad \text{and} \quad F(\boldsymbol{v}) = F(|\boldsymbol{v}|). \tag{42}$$

The coefficient of the second term in (41), $T_1[c]$, describes the new favorable direction of the cells and following [14, 15] we assume that $T_1[c](\boldsymbol{v},\boldsymbol{v}') = T_1[c](\boldsymbol{v})$ and consider the positive *taxis* towards the chemoattractant. We then substitute (6), (41) and (42) into the first equation of (5) and neglect $\mathscr{O}(\varepsilon^2)$ terms to obtain the following kinetic chemotaxis system:

$$\begin{cases} \varepsilon f_t + \boldsymbol{v}\cdot\nabla_{\boldsymbol{x}} f = 1 + \dfrac{1}{\varepsilon}\left[(F(\boldsymbol{v}) + \varepsilon T_1)\,\rho - (1+\mathscr{T}_1) f\right], \\ \tau c_t = \alpha\Delta c - \beta c + \gamma\rho, \end{cases} \tag{43}$$

where

$$\mathscr{T}_1(\boldsymbol{x},t) := \int\limits_{\mathscr{V}} \varepsilon T_1[c](\boldsymbol{v})\,\mathrm{d}\boldsymbol{v}. \tag{44}$$

Specific models for turning kernels can be found in the literature. For instance, a group of so-called local models, considered in [15, 71], suggests that $T_1[c]$ depends on point values of c and ∇c and thus (41) takes the form (up to high-order terms):

$$T[c](\boldsymbol{v}) = F(\boldsymbol{v}) + \varepsilon\max(\boldsymbol{v}\cdot\nabla c, 0). \tag{45}$$

Other examples include nonlocal models, where the turning kernel is given by (see, e.g., [14, 15])

$$T[c](\boldsymbol{v}) = \alpha_+\psi(c(\boldsymbol{x},t), c(\boldsymbol{x}+\varepsilon\boldsymbol{v},t)) + \alpha_-\psi(c(\boldsymbol{x},t), c(\boldsymbol{x}-\varepsilon\boldsymbol{v},t)), \tag{46}$$

where ψ is a smooth, positive, nondecreasing function (in the second argument) defined on $\mathbb{R}^+\times\mathbb{R}^+$ and such that $0 < \psi_{\min} \le \psi(c,\tilde{c}) \le \alpha_1\tilde{c} + \alpha_2$ with $\alpha_+, \alpha_-, \alpha_1$ and α_2 being some positive constants. This model implies that the cell is able to measure the chemoattractant concentration up to a distance $\varepsilon\boldsymbol{v}_{\max}$ away from its position, where $\boldsymbol{v}_{\max}$ is the maximal speed in $\mathscr{V}$. A simplified version of (46) with

$\alpha_+ = 1, \alpha_- = 0$ and $\psi(c,\tilde{c}) = \max(\tilde{c}-c,0)$ was considered in [14] and reads as

$$T[c](\boldsymbol{v}) = F(\boldsymbol{v}) + \max\left(c(\boldsymbol{x}+\varepsilon\boldsymbol{v},t) - c(\boldsymbol{x},t), 0\right). \tag{47}$$

In both models (45) and (47), the turning probability is higher for a change to a favorable direction and away from an unfavorable direction.

In what follows we describe an AP method for the system (43) following the idea of an odd-even formulation, which was first presented in [50] and further developed in [14,19]. Such formulation allows one to efficiently implement the Strang splitting approach [83], by separating stiff and nonstiff parts of the system. In this setup, the nonstiff subsystem reduces to a system of linear transport equations, which can be solved by a second-order upwind method, and the stiff subsystem may either be solved exactly or by an implicit (uniformly stable in ε) method. The resulting numerical method becomes AP in the sense that it yields an accurate and uniformly stable in ε discretization, which stays consistent with the limiting system as $\varepsilon \to 0$.

3.1 Odd-Even Formulation

We restrict our attention to spherically symmetric sets $\mathscr{V} := \{\boldsymbol{v},\ |\boldsymbol{v}| = v_0\}$ as a typical example and denote by $\mathscr{V}^+ := \{\boldsymbol{v} = (u,v) \in \mathscr{V} \,|\, u > 0, v > 0\}$. From now on, we consider $\boldsymbol{v} \in \mathscr{V}^+$ only and introduce new variables r_1, j_1, r_2 and j_2:

$$\begin{aligned}
r_1(u,v) &= R_1[f] := \frac{1}{2}[f(u,-v) + f(-u,v)],\\
r_2(u,v) &= R_2[f] := \frac{1}{2}[f(u,v) + f(-u,-v)],\\
j_1(u,v) &= J_1[f] := \frac{1}{2\varepsilon}[f(u,-v) - f(-u,v)],\\
j_2(u,v) &= J_2[f] := \frac{1}{2\varepsilon}[f(u,v) - f(-u,-v)],
\end{aligned} \tag{48}$$

with a one-to-one correspondence between them and f:

$$f(u,v) = \begin{cases} r_2 + \varepsilon j_2, & u > 0,\ v > 0,\\ r_2 - \varepsilon j_2, & u < 0,\ v < 0,\\ r_1 + \varepsilon j_1, & u > 0,\ v < 0,\\ r_1 - \varepsilon j_1, & u < 0,\ v > 0. \end{cases}$$

It is instructive to point out that the macroscopic cell density ρ can be obtained from (6) and (48) in terms of the new variables r_1 and r_2:

$$\rho(\boldsymbol{x},t) = 2\int\limits_{\mathscr{V}^+} [r_1(\boldsymbol{x},t,\boldsymbol{v}) + r_2(\boldsymbol{x},t,\boldsymbol{v})]\,\mathrm{d}\boldsymbol{v}. \tag{49}$$

Using for simplicity the notation $f(\pm u,\pm v)$ instead of $f(\boldsymbol{x},t,\pm u,\pm v)$ and $T_1(\pm u,\pm v)$ instead of $T_1[c](\boldsymbol{x},t,\pm u,\pm v)$ and taking into account that

$$
\begin{aligned}
&\varepsilon f_t(u,v)+uf_x(u,v)+vf_y(u,v)\\
&\qquad=\frac{\rho}{\varepsilon}\left[F(u,v)+\varepsilon T_1(u,v)\right]-\frac{1}{\varepsilon}\left(1+\mathscr{T}_1\right)f(u,v),\\
&\varepsilon f_t(-u,-v)-uf_x(-u,-v)-vf_y(-u,-v)\\
&\qquad=\frac{\rho}{\varepsilon}\left[F(-u,-v)+\varepsilon T_1(-u,-v)\right]-\frac{1}{\varepsilon}\left(1+\mathscr{T}_1\right)f(-u,-v),\\
&\varepsilon f_t(u,-v)+uf_x(u,-v)-vf_y(u,-v)\\
&\qquad=\frac{\rho}{\varepsilon}\left[F(u,-v)+\varepsilon T_1(u,-v)\right]-\frac{1}{\varepsilon}\left(1+\mathscr{T}_1\right)f(u,-v),\\
&\varepsilon f_t(-u,v)-uf_x(-u,v)+vf_y(-u,v)\\
&\qquad=\frac{\rho}{\varepsilon}\left[F(-u,v)+\varepsilon T_1(-u,v)\right]-\frac{1}{\varepsilon}\left(1+\mathscr{T}_1\right)f(-u,v),
\end{aligned}
$$

we rewrite the first equation in (43) as a system of the following four coupled equations for r_1, j_1, r_2 and j_2:

$$
\begin{aligned}
&(r_1)_t+u(j_1)_x-v(j_1)_x=\frac{\rho}{\varepsilon^2}\left(F(u,v)+\varepsilon R_1[T_1]\right)-\frac{1}{\varepsilon^2}\left(1+\mathscr{T}_1\right)r_1,\\
&(j_1)_t+\frac{1}{\varepsilon^2}u(r_1)_x-\frac{1}{\varepsilon^2}v(r_1)_y=\frac{\rho}{\varepsilon}J_1[T_1]-\frac{1}{\varepsilon^2}\left(1+\mathscr{T}_1\right)j_1,\\
&(r_2)_t+u(j_2)_x+v(j_2)_y=\frac{\rho}{\varepsilon^2}\left(F(u,v)+\varepsilon R_2[T_1]\right)-\frac{1}{\varepsilon^2}\left(1+\mathscr{T}_1\right)r_2,\\
&(j_2)_t+\frac{1}{\varepsilon^2}u(r_2)_x+\frac{1}{\varepsilon^2}v(r_2)_y=\frac{\rho}{\varepsilon}J_2[T_1]-\frac{1}{\varepsilon^2}\left(1+\mathscr{T}_1\right)j_2.
\end{aligned}
\tag{50}
$$

Since the left-hand sides of the second and fourth equations in (50) include stiff terms with the $\dfrac{1}{\varepsilon^2}$ coefficients, we add and subtract $u(r_1)_x-v(r_1)_y$ and $u(r_2)_x+v(r_2)_y$ from the second and fourth equations, respectively, so that we finally replace the system (43) with the following system for r_1,j_1,r_2,j_2 and c:

$$\begin{cases} (r_1)_t + u(j_1)_x - v(j_1)_x = \dfrac{\rho}{\varepsilon^2}\left(F(u,v) + \varepsilon R_1[T_1]\right) - \dfrac{1}{\varepsilon^2}\left(1+\mathscr{T}_1\right) r_1, \\ (j_1)_t + u(r_1)_x - v(r_1)_y = \dfrac{\rho}{\varepsilon} J_1[T_1] \\ \qquad\quad - \dfrac{1}{\varepsilon^2}\left[(1+\mathscr{T}_1) j_1 + (1-\varepsilon^2) u (r_1)_x - (1-\varepsilon^2) v (r_1)_y\right], \\ (r_2)_t + u(j_2)_x + v(j_2)_y = \dfrac{\rho}{\varepsilon^2}\left(F(u,v) + \varepsilon R_2[T_1]\right) - \dfrac{1}{\varepsilon^2}\left(1+\mathscr{T}_1\right) r_2, \\ (j_2)_t + u(r_2)_x + v(r_2)_y = \dfrac{\rho}{\varepsilon} J_2[T_1] \\ \qquad\quad - \dfrac{1}{\varepsilon^2}\left[(1+\mathscr{T}_1) j_2 + (1-\varepsilon^2) u (r_2)_x + (1-\varepsilon^2) v (r_2)_y\right], \\ \tau c_t = \alpha \Delta c - \beta c + \gamma \rho. \end{cases} \tag{51}$$

Notice that all of the stiff terms in the first four equations in (51) are moved to the RHS.

3.2 Strang Operator Splitting

The idea behind the operating splitting approach is to treat the stiff and nonstiff parts of the system (51) separately. To this end, we first introduce the vector $\boldsymbol{W} := (r_1, j_1, r_2, j_2)^T$ and rewrite the system (51) in the following form:

$$\begin{cases} \boldsymbol{W}_t + A_1 \boldsymbol{W}_x + A_2 \boldsymbol{W}_y = \mathscr{R}, \\ \tau c_t = \alpha \Delta c - \beta c + \gamma \rho, \end{cases}$$

where

$$A_1 = \begin{pmatrix} 0 & u & 0 & 0 \\ u & 0 & 0 & 0 \\ 0 & 0 & 0 & u \\ 0 & 0 & u & 0 \end{pmatrix}, \qquad A_2 = \begin{pmatrix} 0 & -v & 0 & 0 \\ -v & 0 & 0 & 0 \\ 0 & 0 & 0 & v \\ 0 & 0 & v & 0 \end{pmatrix},$$

and

$$\mathscr{R} = \begin{pmatrix} \frac{\rho}{\varepsilon^2}\left(F(u,v) + \varepsilon R_1[T_1]\right) - \frac{1}{\varepsilon^2}\left(1+\mathscr{T}_1\right) r_1 \\ \frac{\rho}{\varepsilon} J_1[T_1] - \frac{1}{\varepsilon^2}\left[(1+\mathscr{T}_1) j_1 + (1-\varepsilon^2) u (r_1)_x - (1-\varepsilon^2) v (r_1)_y\right] \\ \frac{\rho}{\varepsilon^2}\left(F(u,v) + \varepsilon R_2[T_1]\right) - \frac{1}{\varepsilon^2}\left(1+\mathscr{T}_1\right) r_2 \\ \frac{\rho}{\varepsilon} J_2[T_1] - \frac{1}{\varepsilon^2}\left[(1+\mathscr{T}_1) j_2 + (1-\varepsilon^2) u (r_2)_x + (1-\varepsilon^2) v (r_2)_y\right] \end{pmatrix}. \tag{52}$$

We then implement the splitting approach by considering the following two subsystems:

$$\begin{cases} \boldsymbol{W}_t = \mathscr{R}, \\ \tau c_t = 0, \end{cases} \tag{53}$$

and

$$\begin{cases} \boldsymbol{W}_t + A_1 \boldsymbol{W}_x + A_2 \boldsymbol{W}_y = \boldsymbol{0}, \\ \tau c_t = \alpha \Delta c - \beta c + \gamma \rho. \end{cases} \tag{54}$$

We note that in the subsystem (53), only the $\boldsymbol{W}$ variable is evolved in time while c remains unchanged there. It is also instructive to point out that not only c, but also the macroscopic cell density ρ does not change in time in the subsystem (53). Indeed, it follows from (42), (49), (52) and (53) that

$$\begin{aligned} \rho_t = 2 \int\limits_{\mathscr{V}^+} [r_1 + r_2]_t \, \mathrm{d}\boldsymbol{v} = \frac{\rho}{\varepsilon^2} \Bigg[& \int\limits_{\mathscr{V}^+} 4F(\boldsymbol{v}) \, \mathrm{d}\boldsymbol{v} \\ & + \varepsilon \int\limits_{\mathscr{V}^+} \big\{ T_1(u,-v) + T_1(-u,v) + T_1(u,v) + T_1(-u,-v) \big\} \, \mathrm{d}\boldsymbol{v} \Bigg] \\ & - \frac{2}{\varepsilon^2} (1 + \mathscr{T}_1) \int\limits_{\mathscr{V}^+} [r_1 + r_2] \, \mathrm{d}\boldsymbol{v} = 0. \end{aligned} \tag{55}$$

Assuming that the solution at time t is available, we evolve it to the next time level using an operator splitting algorithm, [63, 83, 92], of either the first,

$$\begin{pmatrix} \boldsymbol{W}(\boldsymbol{x}, t + \Delta t, \boldsymbol{v}) \\ c(\boldsymbol{x}, t + \Delta t) \end{pmatrix} \approx \mathscr{L}_2(\Delta t) \mathscr{L}_1(\Delta t) \begin{pmatrix} \boldsymbol{W}(\boldsymbol{x}, t, \boldsymbol{v}) \\ c(\boldsymbol{x}, t) \end{pmatrix}, \tag{56}$$

or second,

$$\begin{pmatrix} \boldsymbol{W}(\boldsymbol{x}, t + \Delta t, \boldsymbol{v}) \\ c(\boldsymbol{x}, t + \Delta t) \end{pmatrix} \approx \mathscr{L}_1(\Delta t/2) \mathscr{L}_2(\Delta t) \mathscr{L}_1(\Delta t/2) \begin{pmatrix} \boldsymbol{W}(\boldsymbol{x}, t, \boldsymbol{v}) \\ c(\boldsymbol{x}, t) \end{pmatrix}, \tag{57}$$

order. Here, $\mathscr{L}_1$ and $\mathscr{L}_2$ stand for numerical solution operators for the stiff and nonstiff subsystems (53) and (54), respectively.

Remark 6. It should be observed that the order of the operators in (56) and (57) is interchangeable.

3.3 Time and Space Discretizations

We now proceed with the description of numerical methods for the subsystems (53) and (54). We consider a computational domain, $\Omega \times \mathscr{V}^+$, where the spatial domain Ω is assumed, as before, to be rectangular and partitioned into uniform Cartesian cells $I_{j,k} := [x_{j-\frac{1}{2}}, x_{j+\frac{1}{2}}] \times [y_{k-\frac{1}{2}}, y_{k+\frac{1}{2}}]$ of size $\Delta x \Delta y$ with the cell centers (x_j, y_k). We also introduce a uniform grid of size $\Delta\theta$ in the velocity domain $\mathscr{V}^+$:

$$\boldsymbol{v}_i = (v_0 \cos\theta_i, v_0 \sin\theta_i), \quad \theta_i = (i - 1/2)\Delta\theta, \tag{58}$$

denote by $F_i := F(\boldsymbol{v}_i)$, $\rho_{j,k}(t) \approx \rho(x_k, y_k, t)$, $c_{j,k}(t) \approx c(x_j, y_k, t)$ and $\boldsymbol{W}_{j,k,i}(t) \approx \boldsymbol{W}(x_j, y_k, t, \boldsymbol{v}_i)$, and assume that the solution $\rho^n_{j,k} = \rho_{j,k}(t^n)$, $c^n_{j,k} = c_{j,k}(t^n)$ and $\boldsymbol{W}^n_{j,k,i} = \boldsymbol{W}_{j,k}(t^n)$ is available at time level $t = t^n$. For simplicity, we will omit the dependence of all of the indexed quantities on time t in the rest of the text, unless it is required for clarity.

3.3.1 $\mathscr{L}_1$: Numerical Solution of the Stiff Subsystem (53)

We start by solving the equations for r_1 and r_2,

$$
\begin{aligned}
(r_1)_t &= \frac{\rho}{\varepsilon^2}\left(F(u,v) + \varepsilon R_1[T_1]\right) - \frac{1}{\varepsilon^2}\left(1 + \mathscr{T}_1\right) r_1, \\
(r_2)_t &= \frac{\rho}{\varepsilon^2}\left(F(u,v) + \varepsilon R_2[T_1]\right) - \frac{1}{\varepsilon^2}\left(1 + \mathscr{T}_1\right) r_2,
\end{aligned}
$$

keeping in mind that both the chemoattractant concentration c and macroscopic density ρ do not change in time during this splitting step as shown in (55). The latter implies that $R_1[T_1]$ and $\mathscr{T}_1$ are also constants in time (as they depend on c and $\boldsymbol{v}$ only) and thus, the semi-discrete approximations for $(r_1)_{j,k,i}$ and $(r_2)_{j,k,i}$,

$$
\begin{aligned}
\frac{\mathrm{d}}{\mathrm{d}t}(r_1)_{j,k,i} + \frac{1}{\varepsilon^2}\left(1 + (\mathscr{T}_1)_{j,k}\right)(r_1)_{j,k,i} &= \frac{\rho_{j,k}}{\varepsilon^2}(F_i + \varepsilon R_1[T_1]_{j,k,i}), \\
\frac{\mathrm{d}}{\mathrm{d}t}(r_2)_{j,k,i} + \frac{1}{\varepsilon^2}\left(1 + (\mathscr{T}_1)_{j,k}\right)(r_2)_{j,k,i} &= \frac{\rho_{j,k}}{\varepsilon^2}(F_i + \varepsilon R_2[T_1]_{j,k,i}),
\end{aligned}
\tag{59}
$$

reduce to the system of linear ODEs, which can be solved exactly. The new point values of r_1 and r_2 are then used to solve the equations for j_1 and j_2:

$$
\begin{aligned}
(j_1)_t &= \frac{\rho}{\varepsilon} J_1[T_1] - \frac{1}{\varepsilon^2}\Big[\left(1 + \mathscr{T}_1\right) j_1 + (1-\varepsilon^2) u\,(r_1)_x - (1-\varepsilon^2) v\,(r_1)_y\Big], \\
(j_2)_t &= \frac{\rho}{\varepsilon} J_2[T_1] - \frac{1}{\varepsilon^2}\Big[\left(1 + \mathscr{T}_1\right) j_2 + (1-\varepsilon^2) u\,(r_2)_x + (1-\varepsilon^2) v\,(r_2)_y\Big].
\end{aligned}
$$

To this end, we use the central differences

$$
\begin{aligned}
((r_m)_x)_{j,k,i} &= \frac{(r_m)_{j+1,k,i} - (r_m)_{j-1,k,i}}{2\Delta x}, \\
((r_m)_y)_{j,k,i} &= \frac{(r_m)_{j,k+1,i} - (r_m)_{j,k-1,i}}{2\Delta y},
\end{aligned}
\qquad m = 1,2,
\tag{60}
$$

and exactly solve the following linear ODEs obtained from a semi-discrete approximations for $(j_1)_{j,k,i}$ and $(j_2)_{j,k,i}$:

$$\begin{aligned}
&\frac{\mathrm{d}}{\mathrm{d}t}(j_1)_{j,k,i}+\frac{1}{\varepsilon^2}(1+(\mathscr{T}_1)_{j,k})(j_1)_{j,k,i}=\\
&\quad -\frac{1}{\varepsilon^2}\Big[(1-\varepsilon^2)u_i((r_1)_x)_{j,k,i}-(1-\varepsilon^2)v_i((r_1)_y)_{j,k,i}\Big]+\frac{\rho_{j,k}}{\varepsilon}J_1[T_1]_{j,k,i},\\
&\frac{\mathrm{d}}{\mathrm{d}t}(j_2)_{j,k,i}+\frac{1}{\varepsilon^2}(1+(\mathscr{T}_1)_{j,k})(j_2)_{j,k,i}=\\
&\quad -\frac{1}{\varepsilon^2}\Big[(1-\varepsilon^2)u_i((r_2)_x)_{j,k,i}+(1-\varepsilon^2)v_i((r_2)_y)_{j,k,i}\Big]+\frac{\rho_{j,k}}{\varepsilon}J_2[T_1]_{j,k,i}.
\end{aligned}\tag{61}$$

3.3.2 $\mathscr{L}_2$: Numerical Solution of the Non-Stiff Subsystem (54)

We first solve the equation for $\boldsymbol{W}$, from which we obtain the macroscopic density ρ and then use it to update the values of the chemoattractant concentration c.

The equation for $\boldsymbol{W}$ can be solved by the second-order upwind method (written here in the semi-discrete form):

$$\begin{aligned}
\frac{\mathrm{d}}{\mathrm{d}t}\boldsymbol{W}_{j,k,i}=&-(A_1^+)_i(\boldsymbol{W}_x^-)_{j,k,i}-(A_1^-)_i(\boldsymbol{W}_x^+)_{j,k,i}\\
&-(A_2^+)_i(\boldsymbol{W}_y^-)_{j,k,i}-(A_2^-)_i(\boldsymbol{W}_y^+)_{j,k,i},
\end{aligned}\tag{62}$$

where

$$(A_1^+)_i=\frac{1}{2}\begin{pmatrix}u_i & u_i & 0 & 0\\ u_i & u_i & 0 & 0\\ 0 & 0 & u_i & u_i\\ 0 & 0 & u_i & u_i\end{pmatrix},\quad (A_1^-)_i=\frac{1}{2}\begin{pmatrix}-u_i & u_i & 0 & 0\\ u_i & -u_i & 0 & 0\\ 0 & 0 & -u_i & u_i\\ 0 & 0 & u_i & -u_i\end{pmatrix},$$

$$(A_2^+)_i=\frac{1}{2}\begin{pmatrix}v_i & -v_i & 0 & 0\\ -v_i & v_i & 0 & 0\\ 0 & 0 & v_i & v_i\\ 0 & 0 & v_i & v_i\end{pmatrix},\quad (A_2^-)_i=\frac{1}{2}\begin{pmatrix}-v_i & -v_i & 0 & 0\\ -v_i & -v_i & 0 & 0\\ 0 & 0 & -v_i & v_i\\ 0 & 0 & v_i & -v_i\end{pmatrix},$$

and

$$\begin{aligned}
(\boldsymbol{W}_x^+)_{j,k,i}&=\frac{-\boldsymbol{W}_{j+2,k,i}+4\boldsymbol{W}_{j+1,k,i}-3\boldsymbol{W}_{j,k,i}}{2\Delta x},\\
(\boldsymbol{W}_x^-)_{j,k,i}&=\frac{3\boldsymbol{W}_{j,k,i}-4\boldsymbol{W}_{j-1,k,i}+\boldsymbol{W}_{j-2,k,i}}{2\Delta x},\\
(\boldsymbol{W}_y^+)_{j,k,i}&=\frac{-\boldsymbol{W}_{j,k+2,i}+4\boldsymbol{W}_{j,k+1,i}-3\boldsymbol{W}_{j,k,i}}{2\Delta y},\\
(\boldsymbol{W}_y^-)_{j,k,i}&=\frac{3\boldsymbol{W}_{j,k,i}-4\boldsymbol{W}_{j,k-1,i}+\boldsymbol{W}_{j,k-2,i}}{2\Delta y},
\end{aligned}$$

are the second-order forward and backward finite-difference approximations of the spatial derivatives. The system of time-dependent ODEs (62) should be numerically integrated in time using a stable and sufficiently accurate ODE solver. It is important to stress that according to the definitions in (48), both r_1 and r_2 (and hence ρ, see

(49)) should be positive, which is not guaranteed unless the ODE solver is used with a very small (possibly impractical) time step Δt. Therefore, one may want to implement a "draining" time step technique described in §2.2; see [19] for details.

Once the new point values of $(r_1)_{j,k,i}$ and $(r_2)_{j,k,i}$ are obtained, they can be used to compute $\rho_{j,k}$ from (49), say, by the midpoint rule:

$$\rho_{j,k} = 2\nu_0 \sum_i \left[(r_1)_{j,k,i} + (r_2)_{j,k,i}\right] \Delta\theta, \quad \forall j,k. \tag{63}$$

Finally, the new point values of the chemoattractant concentration c can be computed by the spectral method using a fast Fourier transform (FFT); see [19] for details.

3.4 AP Property

As it was mentioned in the Introduction, the solutions of the studied kinetic-chemotaxis model is expected to converge to the corresponding solutions of PKS system as $\varepsilon \to 0$. In this section, we repeat the arguments from [19] to show that the numerical method presented in §§3.1–3.3 for (5) provides a consistent discretization of (1) in the limiting $\varepsilon \to 0$ case. This guarantees that the numerical method is AP as the uniform stability in ε is ensured by the fact that the stiff ODEs (59) and (61) are solved exactly.

For simplicity of presentation, we only consider the first-order splitting (56) and either local or nonlocal turning kernels described in (45) and (47), respectively. We denote by

$$\begin{pmatrix} \boldsymbol{W}^* \\ c^* \end{pmatrix} := \mathscr{L}_1(\Delta t) \begin{pmatrix} \boldsymbol{W}^n \\ c^n \end{pmatrix},$$

so that the first-order splitting (56) yields:

$$\begin{pmatrix} \boldsymbol{W}^{n+1} \\ c^{n+1} \end{pmatrix} := \mathscr{L}_2(\Delta t) \begin{pmatrix} \boldsymbol{W}^* \\ c^* \end{pmatrix} = \mathscr{L}_2(\Delta t)\mathscr{L}_1(\Delta t) \begin{pmatrix} \boldsymbol{W}^n \\ c^n \end{pmatrix}.$$

We recall that ρ and c do not change in time during the first splitting step and thus $\rho^*_{j,k} = \rho^n_{j,k}$ and $c^*_{j,k} = c^n_{j,k}$. Also, formulae (45), (47) and (48) imply that $(\mathscr{T}_1)_{j,k} = \mathscr{O}(\varepsilon)$, $\varepsilon J_1[T_1]_{j,k,i} = \mathscr{O}(1)$ and $\varepsilon J_2[T_1]_{j,k,i} = \mathscr{O}(1)$. Using these facts, we obtain that as $\varepsilon \to 0$ the leading terms in (59) and (61) are equal to (see also [14, 19]):

$$(r_1)^*_{j,k,i} = \rho^n_{j,k} F_i, \qquad (r_2)^*_{j,k,i} = \rho^n_{j,k} F_i \tag{64}$$

and

$$
\begin{aligned}
(j_1)^*_{j,k,i} &= \frac{\rho^n_{j,k}(\varepsilon J_1[T_1]^n_{j,k,i}) - u_i((r_1)_x)^*_{j,k,i} + v_i((r_1)_y)^*_{j,k,i}}{1+(\mathscr{T}_1)^n_{j,k}}\\
&= \frac{\rho^n_{j,k}}{2}\Big[u_i(c_x)^n_{j,k} - v_i(c_y)^n_{j,k}\Big] - u_iF_i(\rho_x)^n_{j,k} + v_iF_i(\rho_y)^n_{j,k},\\
(j_2)^*_{j,k,i} &= \frac{\rho^n_{j,k}(\varepsilon J_2[T_1]^n_{j,k,i}) - u_i((r_2)_x)^*_{j,k,i} - v_i((r_2)_y)^*_{j,k,i}}{1+(\mathscr{T}_1)^n_{j,k}}\\
&= \frac{\rho^n_{j,k}}{2}\big[u_i(c_x)_{j,k} + v_i(c_y)_{j,k}\big] - u_iF_i(\rho_x)^n_{j,k} - v_iF_i(\rho_y)^n_{j,k},
\end{aligned}
\tag{65}
$$

respectively, where $(\rho_x)^n_{j,k}$ and $(\rho_y)^n_{j,k}$ are obtained from (60) and (63) and equal to

$$
(\rho_x)^n_{j,k} = \frac{\rho^n_{j+1,k} - \rho^n_{j-1,k}}{2\Delta x}, \qquad (\rho_y)^n_{j,k} = \frac{\rho^n_{j,k+1} - \rho^n_{j,k-1}}{2\Delta y}.
$$

Next, we consider the first and third equations in the semi-discrete upwind scheme (62), which after the forward Euler time discretization read as

$$
\begin{aligned}
\frac{(r_1)^{n+1}_{j,k,i} - (r_1)^*_{j,k,i}}{\Delta t} &= -\frac{1}{2}\Big[u_i((r_1)^-_x)^*_{j,k,i} + u_i((j_1)^-_x)^*_{j,k,i} - u_i((r_1)^+_x)^*_{j,k,i}\\
&\quad + u_i((j_1)^+_x)^*_{j,k,i} + v_i((r_1)^-_y)^*_{j,k,i} - v_i((j_1)^-_y)^*_{j,k,i}\\
&\quad - v_i((r_1)^+_y)^*_{j,k,i} - v_i((j_1)^+_y)^*_{j,k,i}\Big],\\
\frac{(r_2)^{n+1}_{j,k,i} - (r_2)^*_{j,k,i}}{\Delta t} &= -\frac{1}{2}\Big[u_i((r_2)^-_x)^*_{j,k,i} + u_i((j_2)^-_x)^*_{j,k,i}) - u_i((r_2)^+_x)^*_{j,k,i}\\
&\quad + u_i((j_2)^+_x)^*_{j,k,i} + v_i((r_2)^-_y)^*_{j,k,i} + v_i((j_2)^-_y)^*_{j,k,i}\\
&\quad - v_i((r_2)^+_y)^*_{j,k,i} + v_i((j_2)^+_y)^*_{j,k,i}\Big].
\end{aligned}
\tag{66}
$$

Substituting (64) and (65) into (66), adding the above two equations, multiplying by $2v_0\Delta\theta$, summing up over all i and using (63) yield (see [19] for details):

$$
\begin{aligned}
\rho^{n+1}_{j,k} &= \rho^n_{j,k}v_0\sum_i 4F_i\Delta\theta\\
&\quad - v_0\Delta t\Big[(\Delta x)^3(\rho_{xxxx})^n_{j,k}\sum_i u_iF_i\Delta\theta + (\Delta y)^3(\rho_{yyyy})^n_{j,k}\sum_i v_iF_i\Delta\theta\\
&\qquad + 2((\rho c_x)_x)^n_{j,k}\sum_i u_i^2\Delta\theta + 2((\rho c_y)_y)^n_{j,k}\sum_i v_i^2\Delta\theta\\
&\qquad - 4(\rho_{xx})^n_{j,k}\sum_i u_i^2F_i\Delta\theta - 4(\rho_{yy})^n_{j,k}\sum_i v_i^2F_i\Delta\theta\Big].
\end{aligned}
\tag{67}
$$

We finally use (42), (58), and the approximation property of the midpoint rule to establish the following estimates and identities:

$$v_0\sum_i 4F_i\Delta\theta = 1+\mathscr{O}((\Delta\theta)^2),$$

$$v_0\sum_i u_iF_i\Delta\theta \le \frac{v_0^2}{4}+\mathscr{O}((\Delta\theta)^2), \quad v_0\sum_i v_iF_i\Delta\theta \le \frac{v_0^2}{4}+\mathscr{O}((\Delta\theta)^2),$$

$$2v_0\sum_i u_i^2\Delta\theta = 2v_0\sum_i v_i^2\Delta\theta = v_0\sum_i (u_i^2+v_i^2)\Delta\theta = \sum_i v_0^4\Delta\theta \approx \chi,$$

$$4v_0\sum_i u_i^2F_i\Delta\theta = 4v_0\sum_i v_i^2F_i\Delta\theta = 2v_0\sum_i (u_i^2+v_i^2)F_i\Delta\theta = 2\sum_i v_0^4F_i\Delta\theta \approx \mu,$$

which can be used to show that (67) provides a consistent approximation of the first equation in (1).

Acknowledgements A large portion of the material covered in this review is based on the work of the authors with Yekaterina Epshteyn, Hengrui Hu, Mária Lukáčová-Medviďová, Mario Ricchiuto, Şeyma Nur Özcan and Tong Wu, whose valuable contribution we would like to acknowledge here. The work of A. Chertock was supported in part by NSF grants DMS-1521051 and DMS-1818684. The work of A. Kurganov was supported in part by NSFC grant 11771201 and NSF grants DMS-1521009 and DMS-1818666.

References

1. Adler, A.: Chemotaxis in bacteria. Ann. Rev. Biochem. **44**, 341–356 (1975)
2. Alt, W.: Biased random walk models for chemotaxis and related diffusion approximations. J. Math. Biol. **9**(2), 147–177 (1980)
3. Arpaia, L., Ricchiuto, M.: *r*-adaptation for shallow water flows: conservation, well balancedness, efficiency. Comput. & Fluids **160**, 175–203 (2018)
4. Ascher, U.M., Ruuth, S.J., Spiteri, R.J.: Implicit-explicit Runge-Kutta methods for time-dependent partial differential equations. Appl. Numer. Math. **25**(2-3), 151–167 (1997). Special issue on time integration (Amsterdam, 1996)
5. Ascher, U.M., Ruuth, S.J., Wetton, B.T.R.: Implicit-explicit methods for time-dependent partial differential equations. SIAM J. Numer. Anal. **32**(3), 797–823 (1995)
6. Bialké, J., Löwen, H., Speck, T.: Microscopic theory for the phase separation of self-propelled repulsive disks. EPL (Europhysics Letters) **103**(3), 30,008 (2013)
7. Bollermann, A., Noelle, S., Lukáčová-Medviďová, M.: Finite volume evolution Galerkin methods for the shallow water equations with dry beds. Commun. Comput. Phys. **10**(2), 371–404 (2011)
8. Bonner, J.T.: The cellular slime molds, 2nd edn. Princeton University Press, Princeton, New Jersey (1967)
9. Bournaveas, N., Calvez, V.: Critical mass phenomenon for a chemotaxis kinetic model with spherically symmetric initial data **26**(5), 1871–1895 (2009)
10. Budrene, E.O., Berg, H.C.: Complex patterns formed by motile cells of escherichia coli. Nature **349**, 630–633 (1991)
11. Budrene, E.O., Berg, H.C.: Dynamics of formation of symmetrical patterns by chemotactic bacteria. Nature **376**, 49–53 (1995)
12. Calvez, V., Carrillo, J.A.: Volume effects in the Keller-Segel model: energy estimates preventing blow-up. J. Math. Pures Appl. (9) **86**(2), 155–175 (2006)
13. Calvez, V., Perthame, B., Sharifi Tabar, M.: Modified Keller-Segel system and critical mass for the log interaction kernel. In: Stochastic analysis and partial differential equations, *Contemp. Math.*, vol. 429, pp. 45–62. Amer. Math. Soc., Providence, RI (2007)

14. Carrillo, J.A., Yan, B.: An asymptotic preserving scheme for the diffusive limit of kinetic systems for chemotaxis. Multiscale Model. Simul. **11**(1), 336–361 (2013)
15. Chalub, F.A.C.C., Markowich, P.A., Perthame, B., Schmeiser, C.: Kinetic models for chemotaxis and their drift-diffusion limits. Monatsh. Math. **142**(1-2), 123–141 (2004)
16. Chertock, A., Epshteyn, Y., Hu, H., Kurganov, A.: High-order positivity-preserving hybrid finite-volume-finite-difference methods for chemotaxis systems. Adv. Comput. Math. **44**(1), 327–350 (2018)
17. Chertock, A., Fellner, K., Kurganov, A., Lorz, A., Markowich, P.A.: Sinking, merging and stationary plumes in a coupled chemotaxis-fluid model: a high-resolution numerical approach. J. Fluid Mech. **694**, 155–190 (2012)
18. Chertock, A., Kurganov, A.: A positivity preserving central-upwind scheme for chemotaxis and haptotaxis models. Numer. Math. **111**, 169–205 (2008)
19. Chertock, A., Kurganov, A., Lukáčová-Medviďová, M., Özcan, c.N.: An asymptotic preserving scheme for kinetic chemotaxis models in two space dimensions. Kinet. Relat. Models (2018). To appear
20. Chertock, A., Kurganov, A., Ricchiuto, M., Wu, T.: Adaptive moving mesh upwind scheme for the two-species chemotaxis model (2018). Submitted
21. Chertock, A., Kurganov, A., Wang, X., Wu, Y.: On a chemotaxis model with saturated chemotactic flux. Kinet. Relat. Models **5**(1), 51–95 (2012)
22. Childress, S., Percus, J.K.: Nonlinear aspects of chemotaxis. Math. Biosc. **56**, 217–237 (1981)
23. Cohen, M.H., Robertson, A.: Wave propagation in the early stages of aggregation of cellular slime molds. J. Theor. Biol. **31**, 101–118 (1971)
24. Conca, C., Espejo, E., Vilches, K.: Remarks on the blowup and global existence for a two species chemotactic Keller-Segel system in $\mathbb{R}^2$. European J. Appl. Math. **22**(6), 553–580 (2011)
25. Eisenbach, M., Lengeler, J.W., Varon, M., Gutnick, D., Meili, R., Firtel, R.A., Segall, J.E., Omann, G.M., Tamada, A., Murakami, F.: Chemotaxis. Imperial College Press (2004)
26. Epshteyn, Y.: Upwind-difference potentials method for Patlak-Keller-Segel chemotaxis model. J. Sci. Comput. **53**(3), 689–713 (2012)
27. Epshteyn, Y., Izmirlioglu, A.: Fully discrete analysis of a discontinuous finite element method for the Keller-Segel chemotaxis model. J. Sci. Comput. **40**(1-3), 211–256 (2009)
28. Epshteyn, Y., Kurganov, A.: New interior penalty discontinuous galerkin methods for the Keller-Segel chemotaxis model. SIAM J. Numer. Anal. **47**, 386–408 (2008)
29. Espejo, E.E., Stevens, A., Suzuki, T.: Simultaneous blowup and mass separation during collapse in an interacting system of chemotactic species. Differential Integral Equations **25**(3-4), 251–288 (2012)
30. Espejo, E.E., Stevens, A., Velázquez, J.J.L.: A note on non-simultaneous blow-up for a drift-diffusion model. Differential Integral Equations **23**(5-6), 451–462 (2010)
31. Espejo, E.E., Vilches, K., Conca, C.: Sharp condition for blow-up and global existence in a two species chemotactic Keller-Segel system in $\mathbb{R}^2$. European J. Appl. Math. **24**, 297–313 (2013)
32. Espejo Arenas, E.E., Stevens, A., Velázquez, J.J.L.: Simultaneous finite time blow-up in a two-species model for chemotaxis. Analysis (Munich) **29**(3), 317–338 (2009)
33. Fasano, A., Mancini, A., Primicerio, M.: Equilibrium of two populations subject to chemotaxis. Math. Models Methods Appl. Sci. **14**, 503–533 (2004)
34. Filbet, F.: A finite volume scheme for the patlak-keller-segel chemotaxis model. Numer. Math. **104**, 457–488 (2006)
35. Filbet, F., Yang, C.: Numerical simulations of kinetic models for chemotaxis. SIAM J. Sci. Comput. **36**(3), B348–B366 (2014)
36. Gajewski, H., Zacharias, K., Gröger, K.: Global behaviour of a reaction-diffusion system modelling chemotaxis. Mathematische Nachrichten **195**(1), 77–114 (1998)
37. Herrero, M., Velázquez, J.: A blow-up mechanism for a chemotaxis model. Ann. Scuola Normale Superiore **24**, 633–683 (1997)
38. Herrero, M.A., Medina, E., Velázquez, J.: Finite-time aggregation into a single point in a reaction-diffusion system. Nonlinearity **10**(6), 1739 (1997)

39. Herrero, M.A., Velázquez, J.J.: Chemotactic collapse for the iKeller-Segel model. J. Math. Biol. **35**(2), 177–194 (1996)
40. Herrero, M.A., Velázquez, J.J.L.: A blow-up mechanism for a chemotaxis model. Ann. Scuola Normale Superiore **24**, 633–683 (1997)
41. Hillen, T., Othmer, H.G.: The diffusion limit of transport equations derived from velocity-jump processes. SIAM J. Appl. Math. **61**(3), 751–775 (electronic) (2000)
42. Hillen, T., Painter, K.: Global existence for a parabolic chemotaxis model with prevention of overcrowding. Adv. in Appl. Math. **26**(4), 280–301 (2001)
43. Hillen, T., Painter, K.J.: A user's guide to PDE models for chemotaxis. J. Math. Biol. **58**(1-2), 183–217 (2009)
44. Horstmann, D.: From 1970 until now: The Keller-Segel model in chemotaxis and its consequences I. Jahresber. DMV **105**, 103–165 (2003)
45. Horstmann, D.: From 1970 until now: The Keller-Segel model in chemotaxis and its consequences II. Jahresber. DMV **106**, 51–69 (2004)
46. Huang, W., Russell, R.D.: Adaptive moving mesh methods, *Applied Mathematical Sciences*, vol. 174. Springer, New York (2011)
47. Hundsdorfer, W., Ruuth, S.J.: IMEX extensions of linear multistep methods with general monotonicity and boundedness properties. J. Comput. Phys. **225**(2), 2016–2042 (2007)
48. Hwang, H.J., Kang, K., Stevens, A.: Drift-diffusion limits of kinetic models for chemotaxis: a generalization. Discrete Contin. Dyn. Syst. Ser. B **5**(2), 319–334 (2005)
49. Jäger, W., Luckhaus, S.: On explosions of solutions to a system of partial differential equations modelling chemotaxis. Trans. Amer. Math. Soc. **329**(2), 819–824 (1992)
50. Jin, S., Pareschi, L., Toscani, G.: Diffusive relaxation schemes for multiscale discrete-velocity kinetic equations. SIAM J. Numer. Anal. **35**(6), 2405–2439 (electronic) (1998)
51. Keller, E.F., Segel, L.A.: Initiation of slime mold aggregation viewed as an instability. J. Theor. Biol. **26**, 399–415 (1970)
52. Keller, E.F., Segel, L.A.: Model for chemotaxis. J. Theor. Biol. **30**, 225–234 (1971)
53. Keller, E.F., Segel, L.A.: Traveling bands of chemotactic bacteria: A theoretical analysis. J. Theor. Biol. **30**, 235–248 (1971)
54. Kurganov, A., Liu, Y.: New adaptive artificial viscosity method for hyperbolic systems of conservation laws. J. Comput. Phys. **231**, 8114–8132 (2012)
55. Kurganov, A., Lukáčová-Medviďová, M.: Numerical study of two-species chemotaxis models. Discrete Contin. Dyn. Syst. Ser. B **19**, 131–152 (2014)
56. Kurganov, A., Qu, Z., Rozanova, O., Wu, T.: Adaptive moving mesh central-upwind schemes for hyperbolic system of PDEs. Applications to compressible Euler equations and granular hydrodynamics Submitted
57. Kurokiba, M., Ogawa, T.: Finite time blow-up of the solution for a nonlinear parabolic equation of drift-diffusion type. Diff. Integral Eqns **4**, 427–452 (2003)
58. van Leer, B.: Towards the ultimate conservative difference scheme. V. A second-order sequel to Godunov's method. J. Comput. Phys. **32**(1), 101–136 (1979)
59. Levy, D., Requeijo, T.: Modeling group dynamics of phototaxis: from particle systems to PDEs. Discrete Contin. Dyn. Syst. Ser. B **9**(1), 103–128 (electronic) (2008)
60. Lie, K.A., Noelle, S.: On the artificial compression method for second-order nonoscillatory central difference schemes for systems of conservation laws. SIAM J. Sci. Comput. **24**(4), 1157–1174 (2003)
61. Liebchen, B., Löwen, H.: Modelling chemotaxis of microswimmers: from individual to collective behavior. arXiv preprint arXiv:1802.07933 (2018)
62. Lin, C.S., Ni, W.M., Takagi, I.: Large amplitude stationary solutions to a chemotaxis system. J. Differential Equations **72**(1), 1–27 (1988)
63. Marchuk, G.I.: Splitting and alternating direction methods. In: Handbook of numerical analysis, Vol. I, Handb. Numer. Anal., I, pp. 197–462. North-Holland, Amsterdam (1990)
64. Marrocco, A.: 2d simulation of chemotaxis bacteria aggregation. M2AN Math. Model. Numer. Anal. **37**, 617–630 (2003)
65. Nagai, T.: Blowup of nonradial solutions to parabolic-elliptic systems modeling chemotaxis in two-dimensional domains. J. Inequal. Appl. pp. 37–55

66. Nagai, T., Senba, T., Yoshida, K.: Application of the Trudinger-Moser inequality to a parabolic system of chemotaxis. Funkcial. Ekvac. **40**(3), 411–433 (1997)
67. Nanjundiah, V.: Chemotaxis, signal relaying and aggregation morphology. J. Theor. Biol. **42**, 63–105 (1973)
68. Nessyahu, H., Tadmor, E.: Nonoscillatory central differencing for hyperbolic conservation laws. J. Comput. Phys. **87**(2), 408–463 (1990)
69. Ni, W.M.: Diffusion, cross-diffusion, and their spike-layer steady states. Notices Amer. Math. Soc. **45**(1), 9–18 (1998)
70. Othmer, H.G., Dunbar, S.R., Alt, W.: Models of dispersal in biological systems. J. Math. Biol. **26**(3), 263–298 (1988)
71. Othmer, H.G., Hillen, T.: The diffusion limit of transport equations. II. Chemotaxis equations. SIAM J. Appl. Math. **62**(4), 1222–1250 (electronic) (2002)
72. Pareschi, L., Russo, G.: Implicit-Explicit Runge-Kutta schemes and applications to hyperbolic systems with relaxation. J. Sci. Comput. **25**(1-2), 129–155 (2005)
73. Patlak, C.S.: Random walk with persistence and external bias. Bull. Math: Biophys. **15**, 311–338 (1953)
74. Pedley, T.J., Kessler, J.O.: Hydrodynamic phenomena in suspensions of swimming microorganisms. Annu. Rev. Fluid Mech. **24**(1), 313–358 (1992)
75. Perthame, B.: PDE models for chemotactic movements: parabolic, hyperbolic and kinetic. Appl. Math. **49**, 539–564 (2004)
76. Perthame, B.: Transport equations in biology. Frontiers in Mathematics. Birkhäuser Verlag, Basel (2007)
77. Pohl, O., Stark, H.: Dynamic clustering and chemotactic collapse of self-phoretic active particles. Phys. Rev. Lett. **112**(23), 238,303 (2014)
78. Prescott, L.M., Harley, J.P., Klein, D.A.: Microbiology, 3rd edn. Wm. C. Brown Publishers, Chicago, London (1996)
79. Saito, N.: Conservative upwind finite-element method for a simplified Keller-Segel system modelling chemotaxis. IMA J. Numer. Anal. **27**(2), 332–365 (2007)
80. Sleeman, B.D., Ward, M.J., Wei, J.C.: The existence and stability of spike patterns in a chemotaxis model. SIAM J. Appl. Math. **65**(3), 790–817 (electronic) (2005)
81. Stevens, A.: The derivation of chemotaxis equations as limit dynamics of moderately interacting stochastic many-particle systems. SIAM J. Appl. Math. **61**(1), 183–212 (electronic) (2000)
82. Stevens, A., Othmer, H.G.: Aggregation, blowup, and collapse: the ABC's of taxis in reinforced random walks. SIAM J. Appl. Math. **57**(4), 1044–1081 (1997)
83. Strang, G.: On the construction and comparison of difference schemes. SIAM J. Numer. Anal. **5**, 506–517 (1968)
84. Strehl, R., Sokolov, A., Kuzmin, D., Turek, S.: A flux-corrected finite element method for chemotaxis problems. Computational Methods in Applied Mathematics **10**(2), 219–232 (2010)
85. Stroock, D.W.: Some stochastic processes which arise from a model of the motion of a bacterium. Probab. Theory Relat. Fields **28**(4), 305–315 (1974)
86. Sweby, P.K.: High resolution schemes using flux limiters for hyperbolic conservation laws. SIAM J. Numer. Anal. **21**(5), 995–1011 (1984)
87. Tang, H., Tang, T.: Adaptive mesh methods for one- and two-dimensional hyperbolic conservation laws. SIAM J. Numer. Anal. **41**(2), 487–515 (electronic) (2003)
88. Tuval, I., Cisneros, L., Dombrowski, C., Wolgemuth, C.W., Kessler, J.O., Goldstein, R.E.: Bacterial swimming and oxygen transport near contact lines. PNAS **102**, 2277–2282 (2005)
89. Tyson, R., Lubkin, S.R., Murray, J.D.: A minimal mechanism for bacterial pattern formation. Proc. Roy. Soc. Lond. B **266**, 299–304 (1999)
90. Tyson, R., Lubkin, S.R., Murray, J.D.: Model and analysis of chemotactic bacterial patterns in a liquid medium. J. Math. Biol. **38**(4), 359–375 (1999)
91. Tyson, R., Stern, L.G., LeVeque, R.J.: Fractional step methods applied to a chemotaxis model. J. Math. Biol. **41**, 455–475 (2000)

92. Vabishchevich, P.N.: Additive operator-difference schemes. De Gruyter, Berlin (2014). Splitting schemes
93. Velázquez, J.J.L.: Point dynamics in a singular limit of the Keller-Segel model. I. Motion of the concentration regions. SIAM J. Appl. Math. **64**(4), 1198–1223 (electronic) (2004)
94. Velázquez, J.J.L.: Point dynamics in a singular limit of the Keller-Segel model. II. Formation of the concentration regions. SIAM J. Appl. Math. **64**(4), 1224–1248 (electronic) (2004)
95. Wang, X.: Qualitative behavior of solutions of chemotactic diffusion systems: effects of motility and chemotaxis and dynamics. SIAM J. Math. Anal. **31**(3), 535–560 (electronic) (2000)
96. Wolansky, G.: Multi-components chemotactic system in the absence of conflicts. European J. Appl. Math. **13**, 641–661 (2002)
97. Woodward, D., Tyson, R., Myerscough, M., Murray, J., Budrene, E., Berg, H.: Spatio-temporal patterns generated by S. typhimurium. Biophys. J. **68**, 2181–2189 (1995)
98. Yeomans, J.: The hydrodynamics of active systems. In: C.N. Likas, F. Sciortino, E. Zaccarelli, P. Ziherl (eds.) Proceedings of teh INternational School of Physics "Enrico Fermi", pp. 383–415. IOS, Amsterdam, SIF, Bologna (2016)
99. Zhang, X., Shu, C.W.: On maximum-principle-satisfying high order schemes for scalar conservation laws. J. Comput. Phys. **229**(9), 3091–3120 (2010)